

**RAGE in circulating immune cells is fundamental for hippocampal inflammation
and cognitive decline in a mouse model of latent chronic inflammation**

Dasen Ye^{a*}, Akio Miyoshi^{a*}, Tomoe Ushitani^a, Manabu Kadoya^a, Masataka Igeta^b

Kosuke Konishi^a, Takuhito Shoji^a, Koubun Yasuda^c, Shiho Kitaoka^d, Hideshi Yagi^e,

Etsushi Kuroda^c, Yasuhiko Yamamoto^f, Jidong Cheng^{a, g}, Hidenori Koyama^a

^a Department of Diabetes, Endocrinology and Clinical Immunology, ^b Department of Biostatistics, ^c Department of Immunology, ^d Department of Pharmacology, ^e Department of Anatomy and Cell Biology, School of Medicine, Hyogo Medical University, Nishinomiya, Japan

^f Department of Biochemistry and Molecular Biology, Kanazawa University Graduate School of Medical Science, Kanazawa, Japan

^g Department of Endocrinology, Xiang'an Hospital of Xiamen University, Xiamen, China

*These two authors contributed equally to this work.

Running title: RAGE, cognition, and latent chronic inflammation

Corresponding author:

Hidenori Koyama, MD, PhD

Department of Diabetes, Endocrinology and Clinical Immunology, School of Medicine,
Hyogo Medical University

1-1 Mukogawa-cho, Nishinomiya, Hyogo 663-8501, Japan

Tel: +81 798 45 6953; Fax: +81 798 45 6443

E-mail: hkoyama@hyo-med.ac.jp

Abstract

Background: Latent chronic inflammation has been proposed as a key mediator of multiple derangements in metabolic syndrome (MetS), which are increasingly becoming recognized as risk factors for age-related cognitive decline. However, the question remains whether latent chronic inflammation indeed induces brain inflammation and cognitive decline.

Methods: A mouse model of latent chronic inflammation was constructed by a chronic subcutaneous infusion of low dose lipopolysaccharide (LPS) for four weeks. A receptor for advanced glycation end products (RAGE) knockout mouse, a chimeric myeloid cell specific RAGE-deficient mouse established by bone marrow transplantation and a human endogenous secretory RAGE (esRAGE) overexpressing adenovirus system were utilized to examine the role of RAGE in vivo. The cognitive function was examined by a Y-maze test, and the expression level of genes was determined by quantitative RT-PCR, western blot, immunohistochemical staining, or ELISA assays.

Results: Latent chronic inflammation induced MetS features in C57BL/6J mice, which were associated with cognitive decline and brain inflammation characterized by microgliosis, monocyte infiltration and endothelial inflammation, without significant changes in circulating cytokines including TNF- α and IL-1 β . These changes as well as

cognitive impairment were rescued in RAGE knockout mice or chimeric mice lacking RAGE in bone marrow cells. P-selectin glycoprotein ligand-1 (PSGL-1), a critical adhesion molecule, was induced in circulating mononuclear cells in latent chronic inflammation in wild-type but not RAGE knockout mice. These inflammatory changes and cognitive decline induced in the wild-type mice were ameliorated by an adenoviral increase in circulating esRAGE. Meanwhile, chimeric RAGE knockout mice possessing RAGE in myeloid cells were still resistant to cognitive decline and brain inflammation.

Conclusions: These findings indicate that RAGE in inflammatory cells is necessary to mediate stimuli of latent chronic inflammation that cause brain inflammation and cognitive decline, potentially by orchestrating monocyte activation via regulation of PSGL-1 expression. Our results also suggest esRAGE-mediated inflammatory regulation as a potential therapeutic option for cognitive dysfunction in MetS with latent chronic inflammation.

Keyword: Latent chronic inflammation; Peripheral blood mononuclear cells; RAGE/PSGL-1 signaling; Hippocampal inflammation; Cognitive decline; esRAGE

1. Introduction

Lipopolysaccharide (LPS) is a molecule of the membrane of gram-negative bacteria and is well-known to induce endotoxemia with variable inflammatory responses (Benson et al., 2017; Tulkens et al., 2020). Several studies on murine and human models have identified the relationship between obesity and dietary factors, with translocation of LPS into the bloodstream by compromising the gut barrier via microbiota dysbiosis (Caesar et al., 2012; Kalyan et al., 2022; Sato et al., 2014). Mice infused with low dose LPS for four weeks, with the plasma LPS levels similar to mice fed with high-fat diet (HFD), are shown to exhibit body weight increase (Cani et al., 2007), insulin resistance (Anhê et al., 2021), and expressions of inflammatory factors in liver, fat tissue, and muscle (Cani et al., 2007; Iwashita et al., 2013), without altering hemodynamics (Yang et al., 2001). Chronic LPS-infusion also augments the number of infiltrated macrophages and the expression of inflammatory molecules, such as MCP-1 and ICAM-1, in the atherosclerotic lesions from Apoe $-/-$ mice (Li et al., 2016). Thus, chronic low-grade inflammation has been proposed as a key mediator of several derangements observed in metabolic disorders (André et al., 2019; van de Vyver, 2023).

MetS represents risk factors for obesity, diabetes and dementia and patients with MetS have an increased risk of developing Alzheimer disease (Więckowska-Gacek et al., 2021).

A retrospective study demonstrates a link between biomarkers of MetS and rate of cognitive decline among MCI and dementia individuals (Pillai et al., 2023). MetS is characterized by latent chronic inflammation, which is likely to be an underlying mechanism contributing to cognitive impairment (Li et al., 2023). Many animal studies present a wide range of impairments in hippocampus-dependent learning and memory behavior when rodents were fed fat and sugar, which are crucial effects on hippocampal functions (Wang et al., 2022; Yu et al., 2019). These dietary components can increase the permeability of the BBB via not only low-grade inflammation but also multiple factors, including reactive oxygen species (de Aquino et al., 2018; Liu et al., 2021), microbiota dysbiosis (Wu et al., 2023), capillary reduction and pericyte loss (Liu et al., 2023; Liu et al., 2021). Therefore, the question remains how latent chronic inflammation indeed induces brain inflammation and cognitive decline.

Receptor for advanced glycation end-products (RAGE), a pattern recognition receptor, is a multiligand cell surface protein originally isolated from bovine lung (Schmidt et al., 1992). This receptor binds various inflammatory ligands, including N-carboxymethyl-lysine-modified protein (CML / AGE) (Kislinger et al., 1999), high-mobility group box 1 (HMGB1) (Sims et al., 2010), and amyloid- β (A β) (Yan et al., 1996). Therefore, RAGE

is not only involved in AGE-deteriorating activities related to diabetes, but also has an important role in regulation of inflammation. RAGE is expressed in microglia (Origlia et al., 2014), monocytes (Farmer and Kennedy, 2009) and endothelium (Fang et al., 2010), and may boost inflammatory process in the brain. RAGE has also been recognized as a central piece in the pathophysiology of metabolic disorders. We and another group have shown that RAGE knockout mice are protected from adipocyte hypertrophy, obesity and insulin resistance induced by HFD (Monden et al., 2013; Song et al., 2014). We have also reported that RAGE regulates progression of atherosclerosis, endothelial inflammation, and obesity through regulation of inflammatory process (Miyoshi et al., 2019; Monden et al., 2013; Shoji et al., 2006; Ueno et al., 2010).

Soluble RAGE (sRAGE) is the isoform of RAGE which is formed by proteolytic cleavage of RAGE on cell surfaces by metalloproteinase (Zhang et al., 2008). These days, we reported that JNK and ATF4 are two important platforms for TNF- α -stimulated shedding of RAGE (Miyoshi et al., 2019). Endogenous secretory RAGE (esRAGE) is a splice variant that directs synthesis of RAGE proteins that lacks the transmembrane and signaling domain (Yonekura et al., 2003). sRAGE and esRAGE are supposed to work as decoys for RAGE and be protective against AGE-mediated cellular toxicity, as they lack

the intracellular C terminus and transmembrane domain and cannot conduct intracellular signaling (Lamb et al., 2018). The serum sRAGE and esRAGE levels are regarded as a potential protective factor against cognitive decline for APOE ϵ 4 carriers or MCI patients (Chen et al., 2011; Deo et al., 2020). However, it remains to be unelucidated how RAGE signal and decoy system for RAGE are involved in cognitive decline in MetS.

Because of its close relationship with both metabolism and inflammation, we speculated that RAGE orchestrates latent chronic inflammation, intracerebral inflammation, and cognitive decline. The present study was conducted to examine whether latent chronic inflammation triggers cognitive impairment via brain inflammation, in which RAGE signaling plays an important role.

2. MATERIALS AND METHODS

2.1. Animal model of latent chronic inflammation and experimental protocols

The methods used for generation of RAGE targeting construct and RAGE knockout [RAGE ($-/-$)] mice have been described elsewhere (Yamamoto et al., 2001). Animals used in the present experiments were from F2 or F5 backcrosses onto a C57BL/6J genetic background. Wild-type [WT; RAGE ($+/+$)] and RAGE ($-/-$) mice were produced by

mating of RAGE (+/-) mice. Newborns were weaned at four to five weeks of age, housed in SPF cages, and fed a standard pelleted rodent diet. The mice were maintained in a temperature-controlled (24°C) facility with a strict 12-hour light/dark cycle and given free access to food and water. To generate a mouse model of latent chronic inflammation, male mice at 14 weeks of age were anesthetized, and an osmotic mini-pump (Alzet Model 2004) was subcutaneously implanted, as previously described (Cani et al., 2007). The pump was filled with either saline or LPS (*E. coli* 055; B5; L2880, Sigma-Aldrich), and infusion at a dose of 300 µg/kg/day was performed for four weeks. Body weight (BW) and food intake were monitored weekly. The procedures used in this study were approved by the Animal Care and Use Committee of Hyogo Medical University.

After four weeks, spontaneous alteration test was performed and the mice were euthanized, then blood samples were collected from the heart. Serum concentrations of TNF- α , IL-1 β and human soluble RAGE were determined using mouse TNF- α ELISA (MTA00B; R&D Systems), mouse IL-1 β ELISA (MLB00C; R&D Systems) and Human RAGE Quantikine ELISA (DRG00; R&D Systems) kits. White adipose tissues were collected and frozen at -80°C. Other mice were fasted for twelve hours and then glucose levels were measured in blood samples obtained from the tail tip using a glucometer (One touch ultra vue; LifeScan Japan).

2.2. Behavior test

Alternation score, locomotor activity and spatial memory were determined with a Y-maze (40 cm long \times 12 cm wide \times 15 cm high). We chose spontaneous alternation test for working memory analysis based on previous reports with similar methods adapted (Nakamura et al., 2023; Ritzel et al., 2021), and the concept that dentate gyrus activity is shown to be necessary for working memory via connection of prefrontal cortex (Sasaki et al., 2018). For spontaneous alteration test, after introduction into a random arm of the maze, the mouse was allowed to freely explore the three arms for 8 min. The series of arm entries was recorded visually at a distance out of sight from mice in all experiments. In some experiments, we recorded the movements of the mice with web camera (C922n, logicool) and recorded the effects of LPS on the behavior through the computer screen both in C57BL/6J and RAGE ($-/-$) mice. We obtained similar results both with the recording visually and with web camera. Alternation was defined as successive entry into the three arms on overlapping triplet sets. The locomotor activity was defined as the total number of entries. The alternation score (%) was calculated as follows: % Alternation = $[(\text{Number of alternations}) / (\text{Total arm entries} - 2)] \times 100$. The apparatus was wiped with a paper towel between uses and kept clean.

To evaluate spatial memory in some experimental conditions with a previously reported method (Sarnyai et al., 2000), mice were placed into one of the arms of the maze (start arm) and allowed to explore the maze with one of the arms closed for 15 min (training trial). After a 1-hour intertrial interval, mice were returned to the Y maze by placing them in the start arm. Then, the mice were allowed to explore freely all three arms of the maze for 5 min (test trial). The number of entries into and the time spent in each arm, and the first choice of entry were registered from video recordings by an observer blind to the genotype of the mice.

2.3. Quantitative Real-time RT-PCR

Mice organs were stored at -80°C until RNA extraction. Total RNA was extracted from mouse brain with RNeasy Plus Mini kit (74136; QIAGEN) and PBMCs with TRIzol (Invitrogen), then analyzed with NanoDrop (Thermo Fisher Scientific). cDNA was synthesized from the RNA using High Capacity cDNA Reverse Transcription Kit (4368814; Applied Biosystems) and used with TaqMan Universal PCR Master mix (4304437; Applied Biosystems). Ready-to-use specific primers and fluorescence probes (TaqMan Gene Expression Assay) were obtained from Thermo Fisher Scientific and used

according to the manufacturer's protocol. Expression changes were calculated using a comparative Ct method, with the results shown as relative expression standardized based on the expression of eukaryotic 18S rRNA, used as an endogenous reference (4333760F; Applied Biosystems). The following primers were used: IL-6 (Mm00446190_m1), TNF- α (Mm00443258_m1), IL-1 β (Mm00434228_m1), HMGB1 (Mm00849805_gH) and PSGL-1 (Mm01204601_m1).

2.4. Immunohistochemistry

Tissue preparation for immunohistochemistry staining was performed using previously reported methods (Nie et al., 2018). In brief, under deep anesthesia, the mouse was intracardially perfused with phosphate buffered saline (PBS) followed by 0.1M sodium phosphate buffer (pH 7.4) containing 4% paraformaldehyde. The brain was obtained and immersed in 0.1M sodium phosphate buffer (pH 7.4) containing 4% paraformaldehyde and 30% sucrose for 24 hours. After rapid embedding in OCT compound (Sakura Finetek), serial coronal sections with a thickness of 20 μ m were made with a cryostat (Cryostar NX50, Thermo Fisher Scientific). After incubation in blocking buffer with 10% normal donkey serum in PBS containing 0.3% Triton X-100 for 1 hour at room temperature, the sections were then incubated with the following primary antibodies for 24 hours at 4°C:

goat anti-CD31 (AF3628, 1:100; R&D Systems), rabbit anti-Iba-1 (019-19741, 1:2000; WAKO), goat anti-Iba-1 (011-27991, 1:1000; WAKO), rat anti-VCAM1 (CBL1300, 1:200; Sigma-Aldrich), rat anti-CD45 (MCA1388, 1:500; BIO-RAD), FITC anti-mouse CD45.1 (110706, 1:250; BioLegend), APC anti-mouse CD45.2 (109812, 1:250; BioLegend), rabbit anti-PSGL-1 (PA5-81473, 1:2000; Invitrogen) and anti-endogenous secretory RAGE [esRAGE, 1:200; (Shimizu et al., 2020)]. Sections were then incubated with Alexa Fluor 405-, Alexa Fluor 488-, or Alexa Fluor 594-labeled secondary antibodies (donkey anti-goat IgG H&L, ab175664, 1:1000, Abcam; donkey anti-rabbit IgG H&L, A-21206, 1:1000, Invitrogen; donkey anti-rat IgG H&L, A-21209, 1:1000, Invitrogen, respectively) at 4°C for 24 hours. The sections were mounted using VECTASHIELD Hard-Set Mounting Medium with (H-1500) or without (H-1400) DAPI (Vector Laboratories). For quantitative image analysis, digital images at 20X magnification by single focal plane scan were captured from the dentate gyrus (DG) in hippocampus by a confocal laser scanning microscope (LSM780; Carl Zeiss, Germany). Since DG has shown to play a critical role to modulate hippocampal-dependent learning and memory process (Li et al., 2020), we analyzed hippocampal DG in all experiments. For each sample, 3–4 corresponding sections at intervals of 300 µm were collected. For each group, sections from 3 to 5 mice were used for analysis. Each measurement was

expressed as the average of all section measurements per mouse. The number of positive cells in DG in each image was manually quantified. The average values of all sections were taken into the statistical analysis.

2.5. Western blot analysis

Tissues were immediately frozen in liquid nitrogen, and total proteins were extracted using ice-cold lysis buffer II supplemented with 0.5% Nonidet P-40 and a Complete Mini protease inhibitor cocktail (04693124001, Roche), then specific protein expression was determined by western blot analysis as previously described (Monden et al., 2013). The following antibodies were used: rabbit anti-Claudin-5 (ab131259, 1:1000; Abcam), rabbit anti-Zo-1 (61-73001, 1:300; Invitrogen), rabbit anti-VCAM1 (ab134047, 1:1000; Abcam), rabbit anti-ICAM1 (701254, 1:500; Invitrogen), rabbit anti-CCL2/MCP1 (NBP1-07035, 1:1000; Novus Biologicals), rabbit anti- β -actin (4967s, 1:1000; Cell Signaling), rabbit anti-GAPDH (G9545, 1:3000; Sigma-Aldrich), and HRP-conjugated goat anti-rabbit IgG (NA934, 1:2000; Sigma-Aldrich). Protein bands were visualized using an ImageQuant Las 4000 system (GE Healthcare). For quantitative determination of the relative band intensities, protein bands were quantified using Image J software (Packard Instrument Company). The data presented reflects the relative intensity of target protein band to that

of the endogenous control β -actin or GAPDH for each sample.

2.6. Adenovirus-mediated human esRAGE gene transfer in mice

Human esRAGE-expressing pAdHM15-esRAGE (Ad-esRAGE) was prepared as previously described (Shoji et al., 2006). A recombinant adenovirus expressing β -galactosidase (Ad-LacZ) was used as the control. The adenovirus was purified with an Adeno-X Maxi Purification Kit (631532; Takara Bio), with titration determined with an Adeno-X Rapid Titer Kit (632250; Takara Bio), according to the manufacturer's protocol. Either Ad-LacZ or Ad-esRAGE (5.0×10^8 ifu) was intraperitoneally injected to C57BL/6J mice (The Jackson Laboratories, Bar Harbor, ME) at the age of 14 weeks and then injections were repeated once a week.

2.7. Bone marrow transplantation (BMT)

Bone marrow cells were isolated from tibias and femurs of donor mice under sterile conditions. Single cell suspensions prepared from bone marrow isolates were filtered through cell strainers (70 μ m) to remove aggregates and were then washed in PBS. To generate chimeric mice, 8-week-old recipient male CD45.1⁺ RAGE (+/+) or CD45.2⁺ RAGE (-/-) mice were lethally irradiated (5.5 Gy) with two total body exposures 6 hours

apart. Within 24 hours of irradiation, a total of 1×10^7 bone marrow cells isolated from RAGE (+/+) or RAGE (-/-) donors were intravenously injected into recipient mice via the tail vein. Bone marrow reconstitution occurred over six weeks, and successful chimerism (90%) was confirmed by flow cytometry analysis for CD45.1 using vein blood (Akasaki et al., 2016). Bone marrow engraftment in chimeric mice was assessed using FACS-based immunophenotypic analysis of CD45 alloantigen expression profiles of peripheral blood leukocytes [CD45.1-positive recipient mice, CD45.2-positive RAGE (+/+) and RAGE (-/-) donor mice], as previously described in detail (Taut et al., 2008).

2.8. Isolation of mouse peripheral blood mononuclear cells (PBMCs)

Peripheral blood was obtained by cardiac puncture using an EDTA-rinsed syringe, as previously described (Hoggatt et al., 2013). PBMCs were prepared by centrifugation with Lympholyte Mammal Cell Separation Media (CL5110; Cedarlane Laboratories). Subsequently, these cells were collected and used for further real-time RT-PCR analysis, immunostaining, or other in vitro experiments.

2.9. In vitro mouse PBMCs culture

PBMCs were cultured with RPMI-1640 (30263-95; Nacalai Tesque), supplemented with

10% fetal calf serum and 1% penicillin-streptomycin (15140122; Gibco), grown in 6-well plates and incubated with PBS (negative control) or LPS (3 pg/ml and 10 µg/ml). These cells were washed, centrifuged, and collected 24 hours after the treatment, and then the effects on adhesion molecules or inflammatory cytokines were evaluated by real-time RT-PCR.

2.10. Measurement of serum LPS

Serum endotoxin levels were determined by the limulus amebocyte lysate test, which was performed using an Endospecy ES-50M kit (020150; Seikagaku Corporation) according to the manufacturer's instructions.

2.11. Determination of blood brain barrier (BBB) permeability

Influence of LPS-treatment on BBB permeability was determined by measuring Evans blue dye transport across the BBB according to published protocols (Menard et al., 2017). In brief, Evans blue dye (50 mg/kg) was injected intravenously. After 3 h, mice were anesthetized and perfused with PBS and 4% paraformaldehyde to make frozen section. Brains were then cryoprotected in 30% sucrose, frozen and sliced on a cryostat at 30 µm thickness. Sections were stained with CD31 antibody. Evans blue and CD31 signals were

quantified using the ImageJ/Fiji® image analysis software (Schindelin et al., 2012). The estimated values of Evans blue and CD31 were presented as percentage area (% Area) of the micrograph occupied by the respective components of interest.

2.12. Statistical analysis

Values were presented as the mean \pm standard deviation (SD). Comparison between two groups was analyzed using two-tailed unpaired t-test. Group effects were determined by one or two-way ANOVA analysis with Bonferroni correction for multiple comparisons (see table S1-S8). All analyses were performed with JMP software and SAS software version 9.4 (SAS, Cary, NC, USA). Values of $P < 0.05$ were considered to indicate statistical significance.

3. Results

3.1. Latent chronic inflammation evoked cognitive dysfunction, monocyte infiltration, and endothelial inflammation in the hippocampus of C57BL/6J mice.

Continuous low dose LPS-infusion for four weeks is shown to increase plasma endotoxin concentration to similar level in HFD-fed mice, increase BW, and induce insulin resistance (Cani et al., 2007). Consistent with this report, LPS group showed increased

percentage of body weight change as compared with the Control group ($t(34)=3.47$, $P<0.01$) (Figure 1A), while food intake was not significantly different between them (data not shown). There were significant differences between the both groups with respect to other parameters such as epididymal white adipose tissue (eWAT) weight ($t(5)=6.17$, $P<0.01$) and fasting blood glucose ($t(4)=5.12$, $P<0.01$), but not inguinal white adipose tissue (iWAT) weight ($t(5)=0.12$, $P=0.910$) (Figure 1B). In this system, both working memory (Alteration) and spatial memory (Exploring time) evaluated by using a Y-maze, were significantly impaired in the LPS group as compared with the Control group ($t(12)=-4.83$, $P<0.0$, $t(4)=-3.10$, $P<0.05$), without a significant difference in locomotor activity (Total arm entries) (Figure 1C). Levels of the major inflammatory cytokines, TNF- α and IL-1 β , but not IL-6 mRNA, in the hippocampus were significantly higher in the LPS group (TNF- α : $t(14)=2.56$, $P<0.05$, IL-1 β : $t(14)=3.56$, $P<0.01$) (Figure 1D). IL-1 β has been shown to mediate the effects of inflammation on cognition (Youm et al., 2013). Furthermore, the number of Iba-1-positive cells, a type of identified immune cells, in the DG of hippocampus was increased in the LPS as compared with the Control group ($t(8)=8.02$, $P<0.01$) (Figure 1E).

We next examined whether monocyte infiltration into the brain, characterized by Iba-1-

CD45 double-positive cells (Zhang et al., 2012), contributed to inflammation in the hippocampus. Iba-1-CD45 double-positive cells in the hippocampus were increased in the LPS group ($t(8)=6.99$, $P<0.01$) (Figure 1E), suggesting that monocyte infiltration in this subtle chronic inflammatory condition may be involved in cognitive decline. Since hippocampal endothelial inflammation, characterized by elevated VCAM1, can trigger cognitive decline in aged individuals (Yousef et al., 2019), endothelial inflammation in the hippocampus was examined by determining vascular endothelial inflammatory markers with western blot. A significant increase in protein expression was observed for VCAM1 ($t(4)=9.90$, $P<0.01$), but not for ICAM1 or MCP1 (Figure 1F). To examine whether destruction of the BBB might be involved in this process, expression of tight junction proteins in the hippocampus was examined. There were no differences regarding Claudin-5 and Zo-1 protein between the Control and LPS groups (Figure 1G). Continuous low dose LPS-infusion did not increase change in BBB permeability as evident by invariant leakage of Evans blue dye (Figure 1H).

Therefore, monocyte infiltration and endothelial inflammation without marked structural alteration in the BBB are potential mediators of brain inflammation and cognitive dysfunction in the present model of latent chronic inflammation.

3.2. RAGE deletion suppressed cognitive impairment and monocyte infiltration into hippocampus in the model of latent chronic inflammation.

Our previous studies have shown that RAGE is involved in pathophysiological conditions with a background of latent chronic inflammation, including atherosclerosis, obesity and endothelial inflammation (Miyoshi et al., 2019; Monden et al., 2013; Shoji et al., 2006; Ueno et al., 2010). Thus, we speculated that RAGE functions as a scaffold protein to mediate systemic latent inflammation to the brain, and examined whether it regulates brain inflammatory change and/or endothelial inflammation using RAGE ($-/-$) mice. Latent chronic inflammation significantly increased percentage of body weight change relative to the Control in both WT ($t(160)=3.36$, $P<0.05$) and RAGE ($-/-$) mice ($t(160)=2.12$, $P<0.01$) (Figure 2A). Food intake was not significantly different among these four groups (data not shown). Consistent with the previous report (Cani et al., 2007), following LPS treatment, serum endotoxin levels were increased in both the WT ($t(11)=2.76$, $P<0.05$) and RAGE ($-/-$) mice ($t(11)=3.39$, $P<0.01$) without an increase in serum TNF- α and IL-1 β concentrations (Supplementary Figure 1A). Latent chronic inflammation resulted in a significantly decreased working memory (Alteration) and spatial memory (Exploring time) in WT ($t(32)=-5.15$, $P<0.01$, $t(17)=-3.83$, $P<0.01$), but

knocking out RAGE prevented memory impairments ($t(32)=0.01$, $P=0.993$, $t(17)=0.08$, $P=0.937$), with no significant differences in locomotor activity (Total arm entries) between those (Figure 2B). Following LPS-infusion, a significant increase in mRNA level of TNF- α and IL-1 β was observed in the hippocampus of WT (TNF- α ; $t(12)=2.70$, $P<0.05$, IL-1 β ; $t(12)=5.00$, $P<0.01$), but RAGE deficiency abrogated these changes (TNF- α ; $t(12)=0.06$, $P=0.956$, IL-1 β ; $t(12)=0.59$, $P=0.564$) (Figure 2C), which is in line with a previous report showing a role of IL-1 β in cognitive impairment (Cunningham and Sanderson, 2008). No significant LPS-induced changes were found in IL-6 mRNA levels in the hippocampus of WT and RAGE (-/-) mice. Latent chronic inflammation induced monocyte infiltration into the hippocampus of WT ($t(8)=14.68$, $P<0.01$), but lack of RAGE suppressed the change ($t(8)=0.97$, $P=0.359$) (Figure 2D), suggesting that RAGE plays an important role in recruitment of circulating monocytes into the brain during latent chronic inflammation.

3.3. RAGE deficiency protected endothelial inflammation in the hippocampus and monocyte activation in a model of latent chronic inflammation.

We next examined whether RAGE is involved in endothelial inflammation in the brain in latent chronic inflammation. LPS-treatment increased hippocampal VCAM1 protein

expression in WT mice ($t(8)=3.32$, $P<0.05$), whereas no significant change was observed in RAGE ($-/-$) mice ($t(8)=1.39$, $P=0.202$) (Supplementary Figure 1B). LPS-treatment only slightly affected ICAM1 protein expression in both WT and RAGE ($-/-$) mice. Using immunostaining with antibodies against VCAM1 and CD31, inflammatory vascular endothelium in the hippocampus was visualized (Figure 3A). WT mice showed a marked increase in hippocampal inflamed vessels with LPS-infusion ($t(12)=5.74$, $P<0.01$), while RAGE deficiency blocked it ($t(12)=-0.09$, $P=0.932$). A previous report has shown that chronic inflammation stimulated microglia to migrate towards vascular endothelium, which is followed by progression of endothelial inflammation (Haruwaka et al., 2019). We found that inflamed vessels-associated microglia were increased by LPS in WT ($t(12)=5.49$, $P<0.01$), while RAGE deficiency inhibited the change ($t(12)=0.78$, $P=0.448$). Furthermore, no significant differences for BBB tight junction proteins, such as Claudin-5 and Zo-1, were noted between the Control and LPS groups for both WT and RAGE ($-/-$) mice (Supplementary Figure 1C), indicating that changes in BBB tight junction proteins are not the primary mechanisms for latent chronic inflammation-induced cognitive decline. The possibility that monocyte activation could be altered by LPS-treatment through a RAGE-mediated mechanism was also examined. In the present model, there was no change in inflammatory cytokine expressions (TNF- α , IL-1 β and HMGB-1)

in PBMCs in latent chronic inflammation in both WT and RAGE ($-/-$) mice (Supplementary Figure 1D). Of interest, mRNA expression of PSGL-1, a key adhesion molecule for the recruitment of monocytes (Sato et al., 2011), was increased by LPS-treatment in PBMCs in WT ($t(26)=2.98$, $P<0.01$), while no significant change was noted in RAGE ($-/-$) mice ($t(26)=0.17$, $P=0.864$) (Figure 3B), suggesting that monocyte infiltration and hippocampal endothelial inflammation could be associated with the RAGE-dependent change of PSGL-1 in PBMCs. To examine whether PSGL-1-positive monocytes actually migrate across the endothelium into hippocampus, Iba-1, CD45 and PSGL-1 triple-positive cells were examined. A significant increase in number of PSGL-1-positive monocytes was identified in the LPS-WT group ($t(8)=12.52$, $P<0.01$), while RAGE deficiency suppressed it ($t(8)=0.62$, $P=0.553$) (Figure 3C).

3.4. RAGE deletion from myeloid cells improved cognitive decline, decreased monocyte infiltration, and ameliorated hippocampal endothelial inflammation in latent chronic inflammation.

Based on findings indicating that monocyte activation is regulated by RAGE, the association of RAGE expression in immune cells with brain inflammation and cognitive decline was examined. Bone marrow from RAGE ($-/-$) or WT [RAGE ($+/+$)] donor mice

was separately transplanted into CD45.1⁺ recipient mice (Figure 4A). Six weeks following BMT, analysis of peripheral leukocytes taken from chimeric mice revealed an engraftment efficiency >90% (Supplementary Figure 2A). In CD45.1⁺ recipient mice transplanted with WT-bone marrow, LPS-treatment decreased working memory ($t(18)=-5.19$, $P<0.01$), while RAGE-null myeloid cells significantly mitigated LPS-induced cognitive impairment (Alteration) ($t(18)=-0.54$, $P=0.594$), without any changes in locomotor activity (Total arm entries) (Figure 4B). In WT-bone marrow transplanted CD45.1⁺ mice, LPS-treatment increased monocyte infiltration into the hippocampus ($t(8)=7.25$, $P < 0.01$), while RAGE-null myeloid cells significantly attenuated this hippocampal inflammatory process ($t(8)=0$, $P=0.997$) (Figure 4C). LPS-treatment promoted CD45.2 WT donor myeloid cells migration into the hippocampus ($t(8)=20.68$, $P<0.01$), while RAGE deficit CD45.2 donor myeloid cells attenuated the LPS effect ($t(8)=0.41$, $P=0.694$) (Figure 4D). Moreover, in contrast to WT-bone marrow transplanted mice [upper figure: $t(8)=5.03$, $P<0.01$, lower figure: $t(8)=6.08$, $P<0.01$], RAGE-null myeloid cells markedly attenuated endothelial inflammation and associated microglia activation in the hippocampus [upper figure: $t(8)=1.42$, $P=0.577$, lower figure: $t(8)=1.13$, $P=0.292$] (Figure 4E). To identify the origin of vessel-associated microglia, we identified transplanted myeloid cells by CD45.2 immunostaining. There was not much of a

difference in the number of Iba-1, CD45.2 and CD31 positive vessel-associated microglia among the groups (Figure 4F), suggesting that resident microglia also contribute to increase in inflamed vessel-associated microglia.

3.5. Cognitive impairment and monocyte infiltration into hippocampus in latent chronic inflammation were still prevented in RAGE knockout mice transplanted with myeloid cells from RAGE-positive CD45.1+ mice.

To further examine the role of RAGE in monocytes, bone marrow from RAGE-positive CD45.1+ donors was transplanted into RAGE (–/–) CD45.2+ recipient mice (Figure 5A). The effectiveness of CD45.1+ bone marrow engraftment in chimeric CD45.2 RAGE (–/–) recipients was then assessed at six weeks following BMT (Supplementary Figure 2B). Interestingly, even in the presence of RAGE (+/+) immune cells in circulation, LPS-induced impairment of working memory (Alteration) was still protected in RAGE knockout mice ($t(9)=-1.41$, $P=0.193$) (Figure 5B). Associated with the finding, LPS-treatment did not promote monocyte infiltration into hippocampus in this chimeric model ($t(4)=0.49$, $P=0.649$) (Figure 5C). With Iba-1/CD45.1 immunostaining, CD45.1 donor monocytes was not increase in hippocampus by LPS-treatment ($t(4)=0.50$, $P=0.641$) (Figure 5D). In addition, endothelial inflammation and associated microglia in the

hippocampus were not elicited by LPS-treatment ($t(4)=1.52$, $P=0.203$, $t(4)=0.25$, $P=0.814$) (Figure 5E). Vessel-associated CD45.1+ donor myeloid cells also exhibited no significant changes by LPS-treatment ($t(4)=0.19$, $P=0.856$) (Figure 5F). On the other hand, LPS-treatment increased PSGL-1 mRNA expression in PBMCs ($t(5)=2.95$, $P<0.05$) (Figure 5G).

Thus, RAGE in monocytes is necessary but not alone sufficient for hippocampal inflammatory changes and cognitive impairment induced by latent chronic inflammation.

3.6. PSGL-1 expression in circulating inflammatory cells was regulated in a RAGE-dependent manner.

As the above results suggest that RAGE signaling in immune cells might play a key role in this study, we isolated mouse PBMCs to further examine whether RAGE in mononuclear cells is essential for PSGL-1 expression. Since the LPS concentration in serum corresponding to in vivo experiments is assumed to be about 3~5 pg/ml, we used 3 pg/ml LPS to mimic latent chronic inflammation in vitro and compared its effect with high dose (10 $\mu\text{g/mL}$) LPS. LPS at a concentration of 10 $\mu\text{g/mL}$ but not 3 pg/mL upregulated mRNA expressions of TNF- α (vs PBS; $t(7)=6.19$, $P<0.01$, vs 3 pg/mL:

$t(7)=6.13$, $P<0.01$) and IL-1 β (vs PBS; $t(7)=4.54$, $P<0.01$, vs 3 $\mu\text{g/mL}$; $t(7)=4.53$, $P<0.01$) in PBMCs after 24 hours (Figure 6B). However, LPS at both 3 $\mu\text{g/mL}$ ($t(7)=3.43$, $P<0.01$) and 10 $\mu\text{g/mL}$ ($t(7)=7.28$, $P<0.01$) gave a significant increase of PSGL-1 mRNA expressions in PBMCs (Figure 6B). LPS at a concentration of 10 $\mu\text{g/mL}$ significantly upregulated mRNA expressions of TNF- α and IL-1 β in PBMCs from WT (TNF- α ; $t(11)=4.51$, $P<0.01$, IL-1 β ; $t(11)=4.90$, $P<0.01$), RAGE ($-/-$) mice (TNF- α ; $t(11)=5.41$, $P<0.01$, IL-1 β ; $t(11)=6.99$, $P<0.01$) (Figure 6C) and chimeric mice with RAGE ($-/-$) (TNF- α ; $t(5)=3.09$, $P<0.05$, IL-1 β ; $t(5)=3.93$, $P<0.05$) or RAGE ($+/+$) myeloid cells (TNF- α ; $t(6)=3.45$, $P<0.05$, IL-1 β ; $t(6)=3.27$, $P<0.05$) (Figure 6D, E). More importantly, LPS at a concentration of 10 $\mu\text{g/mL}$ markedly upregulated PSGL-1 mRNA in PBMCs from WT mice ($t(10)=7.07$, $P<0.01$), but RAGE deficiency in PBMCs restrained its effect ($t(10)=0.57$, $P=0.578$) (Figure 6C). Likewise, LPS-treatment promoted PSGL-1 mRNA in PBMCs from chimeric mice with RAGE ($+/+$) myeloid cells ($t(6)=2.73$, $P<0.05$), but not from chimeric mice with RAGE ($-/-$) myeloid cells ($t(5)=0.37$, $P=0.730$) (Figure 6D-E), suggesting that LPS-treatment increased PSGL-1 expression in circulating immune cells in a RAGE-dependent manner.

3.7. Adenoviral overexpression of esRAGE rescued cognitive impairment and

inflammatory changes, which were associated with suppression of monocyte PSGL-1 expression related to latent chronic inflammation.

Soluble RAGE (sRAGE) including esRAGE has been shown to be a decoy receptor that can functionally block toxic RAGE signals (Park et al., 1998). The systemic effect of increased serum esRAGE was examined using adenoviral expression system (Shoji et al., 2006). Following a single injection of human esRAGE-overexpressing adenovirus (1.0×10^9 ifu) in C57BL/6J mice, the serum esRAGE concentration was markedly elevated on the first day and remained steadily at a high level until day 3, then showed a slow decrease on day 7 and became undetectable after day 14 (Figure 7A). A human RAGE ELISA system that does not cross-react with mouse RAGE was used for this experiment (Miyoshi et al., 2019), thus the concentration in mouse serum was assumed to be derived from the injected human esRAGE-overexpressing adenovirus. Comparisons of multiple doses of Ad-esRAGE injected (Figure 7A) showed that sRAGE concentration in serum >500 pg/ml was achieved with a dose of 5.0×10^8 ifu, which was greater than the level in serum at 10 hours after a single high dose LPS administration in endothelium-specific human RAGE transgenic mice (Miyoshi et al., 2019). Thus, a dose of 5.0×10^8 ifu was chosen for further experiments. The day before implantation of the osmotic mini-pump, once-weekly injections of Ad-LacZ or Ad-esRAGE into C57BL/6J mice were started (Figure

7B). LPS-treatment impaired working memory in Ad-LacZ-injected mice ($t(20)=-5.92$, $P<0.01$), whereas esRAGE restored the memory ($t(20)=0.42$, $P=0.676$) without any differences in locomotor activity (Figure 7C). Furthermore, LPS-treatment increased monocyte infiltration into the hippocampus in Ad-LacZ-injected mice ($t(8)=11.24$, $P<0.01$), while esRAGE completely abrogated those effects ($t(8)=-0.23$, $P=0.823$) (Figure 7D). Moreover, increased inflamed-vessels, determined with VCAM1 and CD31 immunostaining, ($t(8)=5.27$, $P<0.01$) and inflamed vessel-associated microglia ($t(8)=4.67$, $P<0.01$) noted in the hippocampus of Ad-LacZ-injected mice were markedly attenuated in Ad-esRAGE-injected mice (the former; $t(8)=0.72$, $P=0.490$, the latter; $t(8)=0.39$, $P=0.707$) (Figure 7E). Following Ad-esRAGE injection, esRAGE expression was readily observed in mouse livers (positive control) (Supplementary Figure 3A). Conversely, esRAGE was not observed in the hippocampus in either the Control or under LPS-treated conditions (Supplementary Figure 3B, C). esRAGE immunostaining revealed localization of esRAGE both on the surface and in the cytoplasm of PBMCs (Supplementary Figure 3D). Additionally, PSGL-1 gene expression was increased in PBMCs of Ad-LacZ-injected mice after LPS-treatment ($t(15)=3.92$, $P<0.01$), while esRAGE restrained significant changes ($t(15)=0.10$, $P=0.921$) (Figure 7F). Following LPS-treatment, PSGL-1-positive monocytes in the hippocampus were also increased in

the Ad-LacZ ($t(8)=10.18$, $P<0.01$), but esRAGE suppressed PSGL-1-positive monocytes invasion ($t(8)=0.94$, $P=0.374$) (Figure 7G). Together, these results suggest that increase in serum esRAGE directly works on circulating immune cells, suppresses PSGL-1 expression in these cells, and improves the inflammatory process in the brain. Thus, latent chronic inflammation, a critical part of the pathophysiology of MetS, appears to be deeply involved in cognitive decline via brain inflammation, where RAGE signaling in circulating mononuclear cells plays an essential role.

4. DISCUSSION

Latent chronic inflammation is involved in the pathogenesis of MetS, recognized as a risk factor for cognitive dysfunction, though the mechanism remains largely unknown. Latent chronic inflammation is one of the major hallmarks of MetS, though its pathophysiological role in cognitive decline is poorly understood. To the best of our knowledge, the present findings are the first to show rescue from brain inflammatory changes and cognitive impairment in latent chronic inflammation by suppression of RAGE signaling in circulating inflammatory cells. In addition, RAGE expression in myeloid cells was shown to be essential for brain inflammation and cognitive impairment in this model. Furthermore, the results provide new insight into molecular therapeutic

targets for inhibition of RAGE signaling in circulating mononuclear cells by increasing serum esRAGE.

4.1. RAGE-regulated phenotypical changes in circulating immune cells are necessary but not alone sufficient for hippocampal inflammation and cognitive decline in latent chronic inflammation.

LPS induced brain inflammation and oxidative stress in sepsis model which promoted endothelial inflammation and loss of tight junction, resulting in increase of BBB permeability and cognitive impairment (Haileselassie et al., 2020). As shown in Figure 6B, the response of immune cells was markedly different by LPS concentration. LPS at a concentration of 10 $\mu\text{g/mL}$ (sepsis level) but not 3 pg/mL (LPS level in our mouse model) upregulated mRNA expressions of TNF- α and IL-1 β in PBMCs. Importantly, LPS at 3 pg/mL still upregulated PSGL-1 mRNA in PBMCs. These in vitro results are in close agreement with those of our in vivo experiments (Figure 3B, Supplementary Figure 1D). The causes and progression of obesity and MetS are accompanied by latent chronic inflammation (Saltiel and Olefsky, 2017). Thus, latent chronic inflammation is indeed sufficient to induce circulating immune cell activation, brain inflammation, and cognitive dysfunction.

RAGE is expressed not only in endothelial cells but also in immune cells, such as monocytes (Farmer and Kennedy, 2009) and microglia (Origlia et al., 2014). Thus, it is of great interest to know in which cell RAGE expression is important for brain inflammation and cognitive decline. Increase of inflammatory cytokines in several organs and macrophage infiltration into inflamed tissues were reported in this model (Cani et al., 2007), suggesting circulating immune cells as a primary target of latent chronic inflammation. By using chimeric mice with myeloid cells depleted with RAGE, we showed suppression of RAGE signaling in circulating immune cells is fundamental to mediate brain inflammatory changes and cognitive impairment in latent chronic inflammation. PSGL-1, which belongs to the sialomucin family, has long been investigated as an adhesion molecule implicated in immune cell trafficking across endothelium and is well-documented as a regulator of many aspects of immunological responses by myeloid cells. In addition, PSGL-1 controls the initial tethering of immune cells to activated endothelium. Free-flowing immune cells interaction with endothelium is mediated by the binding of P- and E-selectin, endothelial members of the selectin family, to immune cells PSGL-1 (Ley et al., 2007). Moreover, PSGL-1 is reported to recruit monocytes into inflamed tissues in rodent models of obesity (Sato et al., 2011). Although

high dose LPS (10 $\mu\text{g/mL}$) markedly induced TNF- α and IL-1 β expression in both RAGE (+/+) and RAGE (-/-) mononuclear cells in vitro, LPS at very low concentration (3 pg/ml), which mimics our in vivo experiments, did not induce these changes. Even with these marginal changes in inflammatory markers expressed in mononuclear cells and cytokine levels in serum in the present model, latent chronic inflammation clearly upregulates PSGL-1 expression in circulating immune cells in a RAGE-dependent manner, which potentially contributes to endothelial and brain inflammation, and cognitive decline.

In our model, inflamed endothelium in association of increased VCAM-1 expression in the hippocampus is also dependent on the presence of RAGE. Endothelial inflammation with VCAM-1 induction in the brain is shown to be a promising mediator of cognitive decline (Yousef et al., 2019). Moreover, the present results also showed that RAGE (-/-) mice transplanted with myeloid cells from RAGE+/+ mice were still resistant to the LPS-induced brain inflammatory process, even though LPS treatment increased PSGL-1 mRNA expression in donor myeloid cells. Thus, RAGE expression in brain endothelium may be another target of latent chronic inflammation mediating brain inflammation. RAGE is abundantly expressed in activated endothelium, where it functions as a platform

for leukocyte adhesion and transmigration (Kierdorf and Fritz, 2013). Of importance, in latent chronic inflammation, inflamed endothelium in the hippocampus was significantly attenuated in chimeric mice with RAGE-null bone marrow cells. Furthermore, adenoviral increase in circulating esRAGE, which was not readily detected in brain endothelium (Supplementary Figure 3C), potently suppressed endothelium inflammation in latent chronic inflammation. Taken these results together, endothelial inflammation in the brain seemed to be the consequence of phenotypic change of circulating inflammatory cells in latent chronic inflammation. RAGE-dependent regulation of PSGL-1 in circulating immune cells might be a necessary platform mediating endothelial and hippocampal inflammation in response to latent chronic inflammation.

4.2. Suppression of RAGE signaling by soluble RAGE may be a potential new therapeutic target for inhibiting brain inflammatory process in latent chronic inflammation.

We previously found that TNF- α activated JNK or ATF4 pathways, which are involved in activation of MMP9 and ADAM10, leading to RAGE shedding (Miyoshi et al., 2019). Some cohort studies showed that serum sRAGE level is negatively associated with peripheral A β clearance (Jiang et al., 2018). sRAGE-A β interactions could inhibit A β

neurotoxicity and accelerate A β clearance from brain (Cai et al., 2016). In addition, serum sRAGE level is negatively associated with dementia test score (Wang et al., 2016). Thus, sRAGE may be a predictor and even a potential intervention target for cognitive decline.

We have also reported that low plasma esRAGE is strongly associated with atherosclerosis, MetS, and cardiovascular mortality (Koyama et al., 2007; Koyama et al., 2005). esRAGE is also shown to be positively correlated with cognitive assessment score in type 2 diabetic patients (Chen et al., 2011). Since sRAGE and esRAGE preserve ligand-binding sites, they are assumed to function as decoys for RAGE ligands, leading to blockage of RAGE signaling (Heier et al., 2015). In the present study, increasing serum esRAGE markedly mitigated cognitive impairment as well as brain inflammatory change in latent chronic inflammation. sRAGE can bind to the surface of monocytes, which efficiently inhibits monocyte infiltration into vascular endothelium (Rouhiainen et al., 2004). esRAGE is reported to be widely distributed in tissues, including vascular endothelium, macrophages, and monocytes (Cheng et al., 2005). The present study indicates that serum esRAGE is not directly transported to brain tissues when the BBB is not deteriorated, while it can directly bind to circulating mononuclear cells, and may suppress PSGL-1 expression in response to inflammation.

In conclusion, RAGE may orchestrate a switch of immune cell activation potentially by control of PSGL-1 expression, which may result in promotion of endothelium and brain inflammation and cognitive decline in the presence of latent chronic inflammation. Therapy to increase circulating esRAGE level is a potential novel approach for cognitive dysfunction in latent chronic inflammation.

Limitations of the study

These are several limitations in our study. First, we mainly estimated working memory with Y maze, while spatial memory was examined only in some conditions. Thus, our results may not be sufficient to delineate the effect of LPS and RAGE on hippocampus-dependent spatial memory or general cognitive functions. Thus, future studies that other cognitive parameter by using such as Barnes maze are warranted to provide a more comprehensive understanding the role of RAGE and subtle chronic inflammation in cognitive dysfunction. Second, we visually recorded the movements of the mice at a distance out of sight from mice. To confirm influence of the experimenter, we also recorded behaviors using web camera (logicoool) in some conditions, and obtained similar results as compared with visual recording. However, experimenter influence was not completely negated. Third, a caveat of the present study is that only male mice were

studied. RAGE is induced by 17 beta estradiol through Sp-1 in human vascular endothelial cells (Tanaka et al., 2000). Therefore, we usually use only male mice. However, other researchers have shown that differences in sex may affect the mechanisms between microglia and neuroimmune signaling (Bordt et al., 2020; Lenz and McCarthy, 2015). Finally, although we revealed that PSGL-1⁺ monocytes positively correlated with inflamed-vessels in hippocampus, how monocytes would induce PSGL-1 expression via RAGE signaling and function to regulate endothelial inflammation remains to be further elucidated.

ACKNOWLEDGMENTS

We thank all members of the laboratory for their assistance with the experiments and helpful discussion. This work was supported by a Grant-in-Aid for Graduate Students, Hyogo Medical University (to D.Y.), a Grant-in-Aid for Young Researchers, Hyogo Medical University (to A.M.), a Grant of Hyogo Innovative Challenge grant (to H.K.), and Grants-in-Aid for scientific research from the Japan Society for the Promotion of Science (no. JP20K18914, to A.M.; no. 18K08531, to H.K.). None of the authors have conflicts of interest to declare.

AUTHORS' CONTRIBUTIONS

D. Ye and A. Miyoshi contributed equally to this work.

K. Konishi, S. Kitaoka, and H. Koyama designed the research; M. Kadoya, T. Shoji, and Y. Yamamoto analyzed data; M. Igeta contributed technical statistical analysis; D. Ye, A. Miyoshi, T. Ushitani, and K. Konishi performed experiments; D. Ye, A. Miyoshi, and H. Koyama wrote the manuscript; J. Cheng reviewed the manuscript; and Y. Yamamoto contributed analytic tools; and K. Yasuda, E. Kuroda and H. Yagi contributed experimental methods.

Reference

- Akasaki, S., Matsushita, K., Kato, Y., Fukuoka, A., Iwasaki, N., Nakahira, M., Fujieda, S., Yasuda, K., Yoshimoto, T., 2016. Murine allergic rhinitis and nasal Th2 activation are mediated via TSLP- and IL-33-signaling pathways. *Int Immunol* 28, 65-76.
- André, P., Laugerette, F., Féart, C., 2019. Metabolic Endotoxemia: A Potential Underlying Mechanism of the Relationship between Dietary Fat Intake and Risk for Cognitive Impairments in Humans? *Nutrients* 11.
- Anhê, F.F., Barra, N.G., Cavallari, J.F., Henriksbo, B.D., Schertzer, J.D., 2021. Metabolic endotoxemia is dictated by the type of lipopolysaccharide. *Cell Rep* 36, 109691.
- Benson, S., Engler, H., Wegner, A., Rebernik, L., Spreitzer, I., Schedlowski, M., Elsenbruch, S., 2017. What Makes You Feel Sick After Inflammation? Predictors of Acute and Persisting Physical Sickness Symptoms Induced by Experimental Endotoxemia. *Clin Pharmacol Ther* 102, 141-151.
- Bordt, E.A., Ceasrine, A.M., Bilbo, S.D., 2020. Microglia and sexual differentiation of the developing brain: A focus on ontogeny and intrinsic factors. *Glia* 68, 1085-1099.
- Caesar, R., Reigstad, C.S., Bäckhed, H.K., Reinhardt, C., Ketonen, M., Lundén, G., Cani, P.D., Bäckhed, F., 2012. Gut-derived lipopolysaccharide augments adipose macrophage accumulation but is not essential for impaired glucose or insulin tolerance in mice. *Gut* 61, 1701-1707.
- Cai, Z., Liu, N., Wang, C., Qin, B., Zhou, Y., Xiao, M., Chang, L., Yan, L.J., Zhao, B., 2016. Role of RAGE in Alzheimer's Disease. *Cell Mol Neurobiol* 36, 483-495.
- Cani, P.D., Amar, J., Iglesias, M.A., Poggi, M., Knauf, C., Bastelica, D., Neyrinck, A.M., Fava, F., Tuohy, K.M., Chabo, C., Waget, A., Delmée, E., Cousin, B., Sulpice, T., Chamontin, B., Ferrières, J., Tanti, J.F., Gibson, G.R., Casteilla, L., Delzenne, N.M., Alessi, M.C., Burcelin, R., 2007. Metabolic endotoxemia initiates obesity and insulin resistance. *Diabetes* 56, 1761-1772.
- Chen, G., Cai, L., Chen, B., Liang, J., Lin, F., Li, L., Lin, L., Yao, J., Wen, J., Huang, H., 2011. Serum level of endogenous secretory receptor for advanced glycation end products and other factors in type 2 diabetic patients with mild cognitive impairment. *Diabetes Care* 34, 2586-2590.
- Cheng, C., Tsuneyama, K., Kominami, R., Shinohara, H., Sakurai, S., Yonekura, H., Watanabe, T., Takano, Y., Yamamoto, H., Yamamoto, Y., 2005. Expression profiling of endogenous secretory receptor for advanced glycation end products in human organs. *Mod Pathol* 18, 1385-1396.
- Cunningham, C., Sanderson, D.J., 2008. Malaise in the water maze: untangling the effects

of LPS and IL-1 β on learning and memory. *Brain Behav Immun* 22, 1117-1127.

de Aquino, C.C., Leitão, R.A., Oliveira Alves, L.A., Coelho-Santos, V., Guerrant, R.L., Ribeiro, C.F., Malva, J.O., Silva, A.P., Oriá, R.B., 2018. Effect of Hypoproteic and High-Fat Diets on Hippocampal Blood-Brain Barrier Permeability and Oxidative Stress. *Front Nutr* 5, 131.

Deo, P., Dhillon, V.S., Chua, A., Thomas, P., Fenech, M., 2020. APOE ϵ 4 Carriers Have a Greater Propensity to Glycation and sRAGE Which Is Further Influenced by RAGE G82S Polymorphism. *J Gerontol A Biol Sci Med Sci* 75, 1899-1905.

Fang, F., Lue, L.F., Yan, S., Xu, H., Luddy, J.S., Chen, D., Walker, D.G., Stern, D.M., Schmidt, A.M., Chen, J.X., Yan, S.S., 2010. RAGE-dependent signaling in microglia contributes to neuroinflammation, Abeta accumulation, and impaired learning/memory in a mouse model of Alzheimer's disease. *FASEB J* 24, 1043-1055.

Farmer, D.G., Kennedy, S., 2009. RAGE, vascular tone and vascular disease. *Pharmacol Ther* 124, 185-194.

Haileselassie, B., Joshi, A.U., Minhas, P.S., Mukherjee, R., Andreasson, K.I., Mochly-Rosen, D., 2020. Mitochondrial dysfunction mediated through dynamin-related protein 1 (Drp1) propagates impairment in blood brain barrier in septic encephalopathy. *J Neuroinflammation* 17, 36.

Haruwaka, K., Ikegami, A., Tachibana, Y., Ohno, N., Konishi, H., Hashimoto, A., Matsumoto, M., Kato, D., Ono, R., Kiyama, H., Moorhouse, A.J., Nabekura, J., Wake, H., 2019. Dual microglia effects on blood brain barrier permeability induced by systemic inflammation. *Nat Commun* 10, 5816.

Heier, M., Margeisdottir, H.D., Gaarder, M., Stensæth, K.H., Brunborg, C., Torjesen, P.A., Seljeflot, I., Hanssen, K.F., Dahl-Jørgensen, K., 2015. Soluble RAGE and atherosclerosis in youth with type 1 diabetes: a 5-year follow-up study. *Cardiovasc Diabetol* 14, 126.

Hoggatt, J., Mohammad, K.S., Singh, P., Hoggatt, A.F., Chitteti, B.R., Speth, J.M., Hu, P., Poteat, B.A., Stilger, K.N., Ferraro, F., Silberstein, L., Wong, F.K., Farag, S.S., Czader, M., Milne, G.L., Breyer, R.M., Serezani, C.H., Scadden, D.T., Guise, T.A., Srour, E.F., Pelus, L.M., 2013. Differential stem- and progenitor-cell trafficking by prostaglandin E2. *Nature* 495, 365-369.

Iwashita, M., Nakatsu, Y., Sakoda, H., Fujishiro, M., Kushiya, A., Fukushima, T., Kumamoto, S., Shinjo, T., Kamata, H., Nishimura, F., Asano, T., 2013. Valsartan restores inflammatory response by macrophages in adipose and hepatic tissues of LPS-infused mice. *Adipocyte* 2, 28-32.

Jiang, Y., Shang, S., Li, P., Chen, C., Dang, L., Wang, J., Huo, K., Deng, M., Qu, Q., 2018. Pulse pressure is associated with plasma amyloid- β transport dysfunction. *J Hypertens* 36, 569-579.

Kalyan, M., Tousif, A.H., Sonali, S., Vichitra, C., Sunanda, T., Praveenraj, S.S., Ray, B., Gorantla, V.R., Rungratanawanich, W., Mahalakshmi, A.M., Qoronfleh, M.W., Monaghan, T.M., Song, B.J., Essa, M.M., Chidambaram, S.B., 2022. Role of Endogenous Lipopolysaccharides in Neurological Disorders. *Cells* 11.

Kierdorf, K., Fritz, G., 2013. RAGE regulation and signaling in inflammation and beyond. *J Leukoc Biol* 94, 55-68.

Kislinger, T., Fu, C., Huber, B., Qu, W., Taguchi, A., Du Yan, S., Hofmann, M., Yan, S.F., Pischetsrieder, M., Stern, D., Schmidt, A.M., 1999. N(epsilon)-(carboxymethyl)lysine adducts of proteins are ligands for receptor for advanced glycation end products that activate cell signaling pathways and modulate gene expression. *J Biol Chem* 274, 31740-31749.

Koyama, H., Shoji, T., Fukumoto, S., Shinohara, K., Emoto, M., Mori, K., Tahara, H., Ishimura, E., Kakiya, R., Tabata, T., Yamamoto, H., Nishizawa, Y., 2007. Low circulating endogenous secretory receptor for AGEs predicts cardiovascular mortality in patients with end-stage renal disease. *Arterioscler Thromb Vasc Biol* 27, 147-153.

Koyama, H., Shoji, T., Yokoyama, H., Motoyama, K., Mori, K., Fukumoto, S., Emoto, M., Tamei, H., Matsuki, H., Sakurai, S., Yamamoto, Y., Yonekura, H., Watanabe, T., Yamamoto, H., Nishizawa, Y., 2005. Plasma level of endogenous secretory RAGE is associated with components of the metabolic syndrome and atherosclerosis. *Arterioscler Thromb Vasc Biol* 25, 2587-2593.

Lamb, L.S., Alfonso, H., Norman, P.E., Davis, T.M.E., Forbes, J., Muench, G., Irrgang, F., Almeida, O.P., Golledge, J., Hankey, G.J., Flicker, L., Yeap, B.B., 2018. Advanced Glycation End Products and esRAGE Are Associated With Bone Turnover and Incidence of Hip Fracture in Older Men. *J Clin Endocrinol Metab* 103, 4224-4231.

Lenz, K.M., McCarthy, M.M., 2015. A starring role for microglia in brain sex differences. *Neuroscientist* 21, 306-321.

Ley, K., Laudanna, C., Cybulsky, M.I., Nourshargh, S., 2007. Getting to the site of inflammation: the leukocyte adhesion cascade updated. *Nat Rev Immunol* 7, 678-689.

Li, H., Ren, J., Li, Y., Wu, Q., Wei, J., 2023. Oxidative stress: The nexus of obesity and cognitive dysfunction in diabetes. *Front Endocrinol (Lausanne)* 14, 1134025.

Li, J., Lin, S., Vanhoutte, P.M., Woo, C.W., Xu, A., 2016. Akkermansia Muciniphila Protects Against Atherosclerosis by Preventing Metabolic Endotoxemia-Induced Inflammation in Apoe^{-/-} Mice. *Circulation* 133, 2434-2446.

Li, Y., Bao, H., Luo, Y., Yoan, C., Sullivan, H.A., Quintanilla, L., Wickersham, I., Lazarus, M., Shih, Y.I., Song, J., 2020. Supramammillary nucleus synchronizes with dentate gyrus to regulate spatial memory retrieval through glutamate release. *Elife* 9.

Liu, G., Wang, J., Wei, Z., Fang, C.L., Shen, K., Qian, C., Qi, C., Li, T., Gao, P., Wong, P.C.,

Lu, H., Cao, X., Wan, M., 2023. Elevated PDGF-BB from Bone Impairs Hippocampal Vasculature by Inducing PDGFR β Shedding from Pericytes. *Adv Sci (Weinh)* 10, e2206938.

Liu, Y., Zhang, H., Wang, S., Guo, Y., Fang, X., Zheng, B., Gao, W., Yu, H., Chen, Z., Roman, R.J., Fan, F., 2021. Reduced pericyte and tight junction coverage in old diabetic rats are associated with hyperglycemia-induced cerebrovascular pericyte dysfunction. *Am J Physiol Heart Circ Physiol* 320, H549-H562.

Menard, C., Pfau, M.L., Hodes, G.E., Kana, V., Wang, V.X., Bouchard, S., Takahashi, A., Flanigan, M.E., Aleyasin, H., LeClair, K.B., Janssen, W.G., Labonté, B., Parise, E.M., Lorsch, Z.S., Golden, S.A., Heshmati, M., Tamminga, C., Turecki, G., Campbell, M., Fayad, Z.A., Tang, C.Y., Merad, M., Russo, S.J., 2017. Social stress induces neurovascular pathology promoting depression. *Nat Neurosci* 20, 1752-1760.

Miyoshi, A., Koyama, S., Sasagawa-Monden, M., Kadoya, M., Konishi, K., Shoji, T., Inaba, M., Yamamoto, Y., Koyama, H., 2019. JNK and ATF4 as two important platforms for tumor necrosis factor- α -stimulated shedding of receptor for advanced glycation end products. *FASEB J* 33, 3575-3589.

Monden, M., Koyama, H., Otsuka, Y., Morioka, T., Mori, K., Shoji, T., Mima, Y., Motoyama, K., Fukumoto, S., Shioi, A., Emoto, M., Yamamoto, Y., Yamamoto, H., Nishizawa, Y., Kurajoh, M., Yamamoto, T., Inaba, M., 2013. Receptor for advanced glycation end products regulates adipocyte hypertrophy and insulin sensitivity in mice: involvement of Toll-like receptor 2. *Diabetes* 62, 478-489.

Nakamura, R., Konishi, M., Higashi, Y., Saito, M., Akizawa, T., 2023. Five-mer peptides prevent short-term spatial memory deficits in A β 25-35-induced Alzheimer's model mouse by suppressing A β 25-35 aggregation and resolving its aggregate form. *Alzheimers Res Ther* 15, 83.

Nie, X., Kitaoka, S., Tanaka, K., Segi-Nishida, E., Imoto, Y., Ogawa, A., Nakano, F., Tomohiro, A., Nakayama, K., Taniguchi, M., Mimori-Kiyosue, Y., Kakizuka, A., Narumiya, S., Furuyashiki, T., 2018. The Innate Immune Receptors TLR2/4 Mediate Repeated Social Defeat Stress-Induced Social Avoidance through Prefrontal Microglial Activation. *Neuron* 99, 464-479.e467.

Origlia, N., Criscuolo, C., Arancio, O., Yan, S.S., Domenici, L., 2014. RAGE inhibition in microglia prevents ischemia-dependent synaptic dysfunction in an amyloid-enriched environment. *J Neurosci* 34, 8749-8760.

Park, L., Raman, K.G., Lee, K.J., Lu, Y., Ferran, L.J., Chow, W.S., Stern, D., Schmidt, A.M., 1998. Suppression of accelerated diabetic atherosclerosis by the soluble receptor for advanced glycation endproducts. *Nat Med* 4, 1025-1031.

Pillai, J.A., Bena, J., Bekris, L., Kodur, N., Kasumov, T., Leverenz, J.B., Kashyap, S.R.,

Initiative, A.s.D.N., 2023. Metabolic syndrome biomarkers relate to rate of cognitive decline in MCI and dementia stages of Alzheimer's disease. *Alzheimers Res Ther* 15, 54.

Ritzel, R.M., He, J., Li, Y., Cao, T., Khan, N., Shim, B., Sabirzhanov, B., Aubrecht, T., Stoica, B.A., Faden, A.I., Wu, L.J., Wu, J., 2021. Proton extrusion during oxidative burst in microglia exacerbates pathological acidosis following traumatic brain injury. *Glia* 69, 746-764.

Rouhiainen, A., Kuja-Panula, J., Wilkman, E., Pakkanen, J., Stenfors, J., Tuominen, R.K., Lepäntalo, M., Carpén, O., Parkkinen, J., Rauvala, H., 2004. Regulation of monocyte migration by amphoterin (HMGB1). *Blood* 104, 1174-1182.

Saltiel, A.R., Olefsky, J.M., 2017. Inflammatory mechanisms linking obesity and metabolic disease. *J Clin Invest* 127, 1-4.

Sarnyai, Z., Sibille, E.L., Pavlides, C., Fenster, R.J., McEwen, B.S., Toth, M., 2000. Impaired hippocampal-dependent learning and functional abnormalities in the hippocampus in mice lacking serotonin(1A) receptors. *Proc Natl Acad Sci U S A* 97, 14731-14736.

Sasaki, T., Piatti, V.C., Hwaun, E., Ahmadi, S., Lisman, J.E., Leutgeb, S., Leutgeb, J.K., 2018. Dentate network activity is necessary for spatial working memory by supporting CA3 sharp-wave ripple generation and prospective firing of CA3 neurons. *Nat Neurosci* 21, 258-269.

Sato, C., Shikata, K., Hirota, D., Sasaki, M., Nishishita, S., Miyamoto, S., Kodera, R., Ogawa, D., Tone, A., Kataoka, H.U., Wada, J., Kajitani, N., Makino, H., 2011. P-selectin glycoprotein ligand-1 deficiency is protective against obesity-related insulin resistance. *Diabetes* 60, 189-199.

Sato, J., Kanazawa, A., Ikeda, F., Yoshihara, T., Goto, H., Abe, H., Komiya, K., Kawaguchi, M., Shimizu, T., Ogihara, T., Tamura, Y., Sakurai, Y., Yamamoto, R., Mita, T., Fujitani, Y., Fukuda, H., Nomoto, K., Takahashi, T., Asahara, T., Hirose, T., Nagata, S., Yamashiro, Y., Watada, H., 2014. Gut dysbiosis and detection of "live gut bacteria" in blood of Japanese patients with type 2 diabetes. *Diabetes Care* 37, 2343-2350.

Schindelin, J., Arganda-Carreras, I., Frise, E., Kaynig, V., Longair, M., Pietzsch, T., Preibisch, S., Rueden, C., Saalfeld, S., Schmid, B., Tinevez, J.Y., White, D.J., Hartenstein, V., Eliceiri, K., Tomancak, P., Cardona, A., 2012. Fiji: an open-source platform for biological-image analysis. *Nat Methods* 9, 676-682.

Schmidt, A.M., Vianna, M., Gerlach, M., Brett, J., Ryan, J., Kao, J., Esposito, C., Hegarty, H., Hurley, W., Clauss, M., 1992. Isolation and characterization of two binding proteins for advanced glycosylation end products from bovine lung which are present on the endothelial cell surface. *J Biol Chem* 267, 14987-14997.

Shimizu, Y., Harashima, A., Munesue, S., Oishi, M., Hattori, T., Hori, O., Kitao, Y., Yamamoto, H., Leerach, N., Nakada, M., Yamamoto, Y., Hayashi, Y., 2020. Neuroprotective Effects of Endogenous Secretory Receptor for Advanced Glycation End-products in Brain Ischemia.

Aging Dis 11, 547-558.

Shoji, T., Koyama, H., Morioka, T., Tanaka, S., Kizu, A., Motoyama, K., Mori, K., Fukumoto, S., Shioi, A., Shimogaito, N., Takeuchi, M., Yamamoto, Y., Yonekura, H., Yamamoto, H., Nishizawa, Y., 2006. Receptor for advanced glycation end products is involved in impaired angiogenic response in diabetes. *Diabetes* 55, 2245-2255.

Sims, G.P., Rowe, D.C., Rietdijk, S.T., Herbst, R., Coyle, A.J., 2010. HMGB1 and RAGE in inflammation and cancer. *Annu Rev Immunol* 28, 367-388.

Song, F., Hurtado del Pozo, C., Rosario, R., Zou, Y.S., Ananthakrishnan, R., Xu, X., Patel, P.R., Benoit, V.M., Yan, S.F., Li, H., Friedman, R.A., Kim, J.K., Ramasamy, R., Ferrante, A.W., Schmidt, A.M., 2014. RAGE regulates the metabolic and inflammatory response to high-fat feeding in mice. *Diabetes* 63, 1948-1965.

Tanaka, N., Yonekura, H., Yamagishi, S., Fujimori, H., Yamamoto, Y., Yamamoto, H., 2000. The receptor for advanced glycation end products is induced by the glycation products themselves and tumor necrosis factor- α through nuclear factor- κ B, and by 17 β -estradiol through Sp-1 in human vascular endothelial cells. *J Biol Chem* 275, 25781-25790.

Taut, K., Winter, C., Briles, D.E., Paton, J.C., Christman, J.W., Maus, R., Baumann, R., Welte, T., Maus, U.A., 2008. Macrophage Turnover Kinetics in the Lungs of Mice Infected with *Streptococcus pneumoniae*. *Am J Respir Cell Mol Biol* 38, 105-113.

Tulkens, J., Vergauwen, G., Van Deun, J., Geeurickx, E., Dhondt, B., Lippens, L., De Scheerder, M.A., Miinalainen, I., Rappu, P., De Geest, B.G., Vandecasteele, K., Laukens, D., Vandekerckhove, L., Denys, H., Vandesompele, J., De Wever, O., Hendrix, A., 2020. Increased levels of systemic LPS-positive bacterial extracellular vesicles in patients with intestinal barrier dysfunction. *Gut* 69, 191-193.

Ueno, H., Koyama, H., Shoji, T., Monden, M., Fukumoto, S., Tanaka, S., Otsuka, Y., Mima, Y., Morioka, T., Mori, K., Shioi, A., Yamamoto, H., Inaba, M., Nishizawa, Y., 2010. Receptor for advanced glycation end-products (RAGE) regulation of adiposity and adiponectin is associated with atherogenesis in apoE-deficient mouse. *Atherosclerosis* 211, 431-436.

van de Vyver, M., 2023. Immunology of chronic low-grade inflammation: relationship with metabolic function. *J Endocrinol* 257.

Wang, J., Li, L., Zhang, Z., Zhang, X., Zhu, Y., Zhang, C., Bi, Y., 2022. Extracellular vesicles mediate the communication of adipose tissue with brain and promote cognitive impairment associated with insulin resistance. *Cell Metab* 34, 1264-1279.e1268.

Wang, P., Huang, R., Lu, S., Xia, W., Cai, R., Sun, H., Wang, S., 2016. RAGE and AGEs in Mild Cognitive Impairment of Diabetic Patients: A Cross-Sectional Study. *PLoS One* 11, e0145521.

Więkowska-Gacek, A., Mietelska-Porowska, A., Wydrych, M., Wojda, U., 2021. Western diet

as a trigger of Alzheimer's disease: From metabolic syndrome and systemic inflammation to neuroinflammation and neurodegeneration. *Ageing Res Rev* 70, 101397.

Wu, H., Zhang, W., Huang, M., Lin, X., Chiou, J., 2023. Prolonged High-Fat Diet Consumption throughout Adulthood in Mice Induced Neurobehavioral Deterioration via Gut-Brain Axis. *Nutrients* 15.

Yamamoto, Y., Kato, I., Doi, T., Yonekura, H., Ohashi, S., Takeuchi, M., Watanabe, T., Yamagishi, S., Sakurai, S., Takasawa, S., Okamoto, H., Yamamoto, H., 2001. Development and prevention of advanced diabetic nephropathy in RAGE-overexpressing mice. *J Clin Invest* 108, 261-268.

Yan, S.D., Chen, X., Fu, J., Chen, M., Zhu, H., Roher, A., Slattery, T., Zhao, L., Nagashima, M., Morser, J., Migheli, A., Nawroth, P., Stern, D., Schmidt, A.M., 1996. RAGE and amyloid-beta peptide neurotoxicity in Alzheimer's disease. *Nature* 382, 685-691.

Yang, S., Zhou, M., Chaudry, I.H., Wang, P., 2001. The role of lipopolysaccharide in stimulating adrenomedullin production during polymicrobial sepsis. *Biochim Biophys Acta* 1537, 167-174.

Yonekura, H., Yamamoto, Y., Sakurai, S., Petrova, R.G., Abedin, M.J., Li, H., Yasui, K., Takeuchi, M., Makita, Z., Takasawa, S., Okamoto, H., Watanabe, T., Yamamoto, H., 2003. Novel splice variants of the receptor for advanced glycation end-products expressed in human vascular endothelial cells and pericytes, and their putative roles in diabetes-induced vascular injury. *Biochem J* 370, 1097-1109.

Youn, Y.H., Grant, R.W., McCabe, L.R., Albarado, D.C., Nguyen, K.Y., Ravussin, A., Pistell, P., Newman, S., Carter, R., Laque, A., Münzberg, H., Rosen, C.J., Ingram, D.K., Salbaum, J.M., Dixit, V.D., 2013. Canonical Nlrp3 inflammasome links systemic low-grade inflammation to functional decline in aging. *Cell Metab* 18, 519-532.

Yousef, H., Czupalla, C.J., Lee, D., Chen, M.B., Burke, A.N., Zera, K.A., Zandstra, J., Berber, E., Lehallier, B., Mathur, V., Nair, R.V., Bonanno, L.N., Yang, A.C., Peterson, T., Hadeiba, H., Merkel, T., Körbelin, J., Schwaninger, M., Buckwalter, M.S., Quake, S.R., Butcher, E.C., Wyss-Coray, T., 2019. Aged blood impairs hippocampal neural precursor activity and activates microglia via brain endothelial cell VCAM1. *Nat Med* 25, 988-1000.

Yu, M., Huang, H., Dong, S., Sha, H., Wei, W., Liu, C., 2019. High mobility group box-1 mediates hippocampal inflammation and contributes to cognitive deficits in high-fat high-fructose diet-induced obese rats. *Brain Behav Immun* 82, 167-177.

Zhang, L., Bukulin, M., Kojro, E., Roth, A., Metz, V.V., Fahrenholz, F., Nawroth, P.P., Bierhaus, A., Postina, R., 2008. Receptor for advanced glycation end products is subjected to protein ectodomain shedding by metalloproteinases. *J Biol Chem* 283, 35507-35516.

Zhang, X., Wang, B., O'Callaghan, P., Hjertström, E., Jia, J., Gong, F., Zcharia, E., Nilsson,

L.N., Lannfelt, L., Vlodavsky, I., Lindahl, U., Li, J.P., 2012. Heparanase overexpression impairs inflammatory response and macrophage-mediated clearance of amyloid- β in murine brain. *Acta Neuropathol* 124, 465-478.

Figure Legends

Figure 1. Latent chronic inflammation induced cognitive impairment, monocyte infiltration, and hippocampal endothelium inflammation.

A. Schematic illustration of the latent chronic inflammation mouse model. Body weight in C57BL/6J mice before (week 0) and after 4-week treatment period (week 4).

Percentage of body weight change is shown as body weight in week 4 relative to that in week 0 (n=16-20/group). White circles: Control group, black circles: LPS group

B. Inguinal (iWAT) and epididymal white adipose tissue (eWAT) weight (percentage of body weight) and fasting blood glucose (mmol/l) (n=3-5/group)

C. Assessment of working memory (Alteration) and locomotor activity (total arm entries, right panel) with Y-maze test (n=6-8/group). Spatial memory performance was evaluated in the Y-maze test by measuring time spent exploring the novel arm (Exploring time, n=3/group).

D. Real-time RT-PCR analysis of TNF- α , IL-6 and IL-1 β mRNA expression levels in the hippocampus (n=4-9/group). Results are shown as relative expression standardized based on expression of eukaryotic 18S rRNA used as the endogenous reference.

E. Representative confocal images in hippocampal DG of monocytes (left panel) determined by Iba-1 (green) and CD45 (red) double-positive cells. Nuclei were

counterstained with DAPI (blue). Scale bar = 50 μ m. Higher magnification inset and arrowheads indicate monocytes. Right panel shows the summary of the quantitative analyses (n=5/group).

F. Western blot and quantification analyses of ICAM1, VCAM1, and MCP1 protein expressions in the hippocampus (n=3-5/group).

G. Western blot and quantification analyses of Claudin-5 and Zo-1 protein expressions in the hippocampus (n=6/group).

H. Representative confocal images of Evans blue (red) with CD31 (blue) for BBB permeability. Scale bar = 50 μ m. Right panel shows the summary of the quantitative analyses (n=3/group).

Values are presented as mean \pm SD. NS: not significant. Statistical analysis was performed by two-tailed unpaired t-test (see table S1).

Figure 2. RAGE deletion restored cognitive impairment and monocyte infiltration into hippocampus in latent chronic inflammation.

A. Body weight in RAGE (+/+) (WT) mice and RAGE (-/-) mice before (week 0) and after 4-week treatment period (week 4). Percentage of body weight change is body weight in week 4 relative to that in week 0 (n=33-48/group). White circles: WT Control group,

black circles: WT LPS group, White squares: RAGE (–/–) Control group, black squares: RAGE (–/–) LPS group.

B. Assessment of cognitive function (Alteration) and locomotor activity (total arm entries) with Y-maze test (n=7-11/group). Spatial memory performance was evaluated in the Y-maze test by measuring time spent exploring the novel arm (Exploring time, n=4-6/group).

C. Relative abundance of TNF- α , IL-6 and IL-1 β mRNA in the hippocampus, determined by real-time RT-PCR analysis (n=3-6/group). Results are shown as relative expression standardized based on expression of eukaryotic 18S rRNA endogenous reference.

D. Representative confocal images and quantitative analyses in the hippocampal DG of Iba-1 (green), CD45 (red) and DAPI (blue) staining (n=3/group). DAPI labeled cell nuclei. Higher magnification inset and arrowheads indicate monocytes, co-immunodetection of Iba-1 and CD45 double-positive cells. Scale bar = 50 μ m. Right panel shows the summary of the quantitative analyses (n=3/group). Values are presented as mean \pm SD. NS: not significant. Statistical analysis was performed by two-way ANOVA with Bonferroni correction for multiple comparisons (see table S2).

Figure 3. Endothelial inflammation and monocyte activation with increased RAGE-

dependent PSGL-1 expression in latent chronic inflammation.

A. Representative confocal images in the hippocampal DG area of Iba-1 (green), VCAM1 (red) and CD31 (blue) staining. Colocalization of CD31 and VCAM1 indicates inflamed vessels. Inflamed vessel-associated microglia are represented by Iba-1-positive cells in close contact with the inflamed vessels. Higher magnification inset and arrowheads indicate the inflamed vessel-associated microglia. Scale bar = 50 μ m. Right panel shows the summary of the quantitative analyses (n=4/group).

B. Real-time RT-PCR analysis of PSGL-1 mRNA expression standardized by expression of the eukaryotic 18S rRNA endogenous reference in PBMCs (n=5-10/group).

C. Representative confocal images in the DG of brain sections for Iba-1 (green), CD45 (red) and PSGL-1 (blue) staining. Higher magnification inset and arrowheads show PSGL-1-positive monocytes. Scale bar = 50 μ m. Right panel shows the summary of the quantitative analyses (n=4/group). Values are shown as mean \pm SD. NS: not significant. Statistical analysis was performed by two-way ANOVA with Bonferroni correction for multiple comparisons (see table S3).

Figure 4. Transplantation of myeloid cells from RAGE knockout mice improved cognitive impairment and hippocampal inflammation in latent chronic

inflammation.

A. The experimental schedule of the chimeric model study with bone marrow transplanted from RAGE (–/–) or RAGE (+/+) (WT) donors into CD45.1+ recipient mice.

B. Assessment of cognition (Alteration) and locomotor activity (total arm entries) with Y-maze test (n=5-6/group).

C. Representative results of confocal microscope analysis (left panel) of monocytes using co-immunodetection of Iba-1 (green) and CD45 (red) positive cells in the hippocampal DG. Nuclei were stained with DAPI (blue). Higher magnification inset and arrowheads indicate monocytes. Scale bar = 50µm. Right panel shows the summary of the quantitative analyses (n=3/group).

D. Representative photomicrographs and quantification in the DG of CD45.2 donor monocytes, defined by Iba-1 (green)-CD45.2 (red) positive cells. Higher magnification inset and arrowheads indicate CD45.2 donor monocytes. Scale bar = 50µm. Right panel shows the summary of the quantitative analyses (n=3/group).

E. Representative confocal images in the hippocampal DG of brain sections for inflamed vessels, determined by VCAM1 (red) and CD31 (blue) staining. Inflamed vessel-associated microglia were shown by Iba-1-positive cells (green) in close contact with the inflamed vessels. Higher magnification inset and arrowheads indicate the inflamed

vessel-associated microglia. Scale bar = 50 μ m. Right panel shows the summary of the quantitative analyses (n=3/group).

F. Typical images in the hippocampal DG for vessel-associated CD45.2 donor myeloid cells, determined by Iba-1 (green), CD45.2 (red) and CD31 (blue) staining. Higher magnification inset and arrowheads indicate the inflamed vessel-associated monocytes.

Scale bar = 50 μ m. Right panel shows the summary of the quantitative analyses (n=3/group). Values are shown as mean \pm SD. NS: not significant. Statistical analysis was performed by two-way ANOVA with Bonferroni correction for multiple comparisons (see table S4).

Figure 5. RAGE ($-/-$) mice transplanted with myeloid cells from WT mice did not display cognitive impairment or inflammatory response in latent chronic inflammation.

A. Schematic illustration of the chimeric model with bone marrow transplanted from RAGE (+/+) CD45.1+ donors to RAGE ($-/-$) recipients.

B. Assessment of working memory (Alteration) and locomotor activity (total arm entries) with Y-maze test (n=5-6/group).

C. Representative photomicrographs and quantification in the hippocampal DG of

monocytes, defined by Iba-1 (green)-CD45 (red) positive cells. Nuclei were stained with DAPI (blue). Higher magnification inset and arrowheads indicate monocytes. Scale bar = 50 μ m. Right panel shows the summary of the quantitative analyses (n=3/group).

D. Representative images in the hippocampal DG of CD45.1+ donor monocytes, identified by Iba-1 (green)-CD45.1 (red) positive cells. Higher magnification inset and arrowheads indicate CD45.1+ donor monocytes. Scale bar = 50 μ m. Right panel shows the summary of the quantitative analyses (n=3/group).

E. Typical confocal images and quantitative analyses in the hippocampal DG of co-immunodetection for Iba-1 (green), VCAM1 (red) and CD31 (blue). Higher magnification inset indicates VCAM1+ vessel-associated microglia. Scale bar = 50 μ m. Right panel shows the summary of the quantitative analyses (n=3/group).

F. Immunohistochemistry and quantification of vessel-associated CD45.1+ donor myeloid cells in the DG, determined by Iba-1 (green), CD45.1 (red) and CD31 (blue) staining. Higher magnification inset indicates CD45.1+ donor monocytes. Scale bar = 50 μ m. Right panel shows the summary of the quantitative analyses (n=3/group).

G. Real-time RT-PCR analysis of PSGL-1 mRNA expression standardized by expression of the eukaryotic 18S rRNA endogenous reference in PBMCs (n=3-4/group).

Values are presented as mean \pm SD. NS: not significant. Statistical analysis was performed

by two-tailed unpaired t-test (see table S5).

Figure 6. LPS-induced PSGL-1 expression in circulating mononuclear cells was regulated in a RAGE-dependent manner.

A. The experimental design of in vitro study.

B. mRNA expressions of adhesion molecules (PSGL-1) and inflammatory cytokines (TNF- α and IL-1 β) in PBMCs from C57BL/6 mice following stimulation with LPS at 3 pg/ml or 10 μ g/ml for 24 hours (n=3-4/group).

C-E. mRNA expressions of PSGL-1, TNF- α and IL-1 β in PBMCs from RAGE (+/+) (WT) mice and RAGE (-/-) mice (C), chimeric mice with RAGE (-/-) (D) and RAGE (+/+) (E) myeloid cells. PBMCs were stimulated with 10 μ g/ml LPS for 24 hours (n=3-5/group). Results are shown as relative expression standardized by expression of eukaryotic 18S rRNA endogenous reference. Values are shown as mean \pm SD. NS: not significant. Statistical analysis was performed by one-way (B) and two-way ANOVA (C) with Bonferroni correction for multiple comparisons and two-tailed unpaired t-test (D-E) (see table S6).

Figure 7. esRAGE rescued hippocampal inflammation, endothelial inflammation,

and cognitive impairment in association with suppression of PSGL-1 expression in circulating mononuclear cells in latent chronic inflammation.

A. Enzyme-linked immunosorbent assay (ELISA) analysis results (left panel) showing time-dependent decrease in serum esRAGE following intraperitoneal injection of single dose of esRAGE-overexpressing adenovirus (1.0×10^9 ifu) in C57BL/6J mice (n=2/group). ELISA analysis results (right panel) showing dose-dependent decrease in serum esRAGE following injection of various doses of esRAGE-overexpressing adenovirus (2.5×10^8 , 5.0×10^8 and 1.0×10^9 ifu) in C57BL/6J mice (n=2/group).

B. The experimental design of the adenoviral system. Fourteen-week-old male C57BL/6J mice received intraperitoneal injections of Ad-LacZ or Ad-esRAGE 1 day prior to implantation of mini-pump, followed by weekly injections for a total of four injections.

C. Assessment of cognitive performance (Alteration) and locomotor activity (total arm entries) with Y-maze test (n=6/group).

D. Representative image showing density of monocytes labeled with Iba-1 (green), CD45 (red) and DAPI (blue) in the hippocampal DG. Scale bar = 50 μ m. Higher magnification inset and arrowheads show monocytes. Bottom panel shows the summary of the quantitative analyses (n=3/group).

E. Representative confocal images in the hippocampal DG of Iba-1 (green), VCAM1

(red) and CD31 (blue) staining. Scale bar = 50 μ m. Higher magnification inset and arrowheads indicate VCAM1+ vessel-associated microglia. Right panel shows the summary of the quantitative analyses (n=3/group).

F. Real-time RT-PCR analysis of PSGL-1 mRNA expression standardized by expression of the eukaryotic 18S rRNA endogenous reference in PBMCs (n=4-6/group).

G. Representative confocal images in the hippocampal DG of the immunostaining for Iba-1 (green), CD45 (red) and PSGL-1 (blue). Scale bar = 50 μ m. Higher magnification inset and arrowheads indicate PSGL-1-positive monocytes. Right panel shows the results of quantitative analyses (n=3/group). Values are shown as mean \pm SD. NS: not significant. Analysis by two-way ANOVA with Bonferroni correction for multiple comparisons (see table S7).

Figure 1

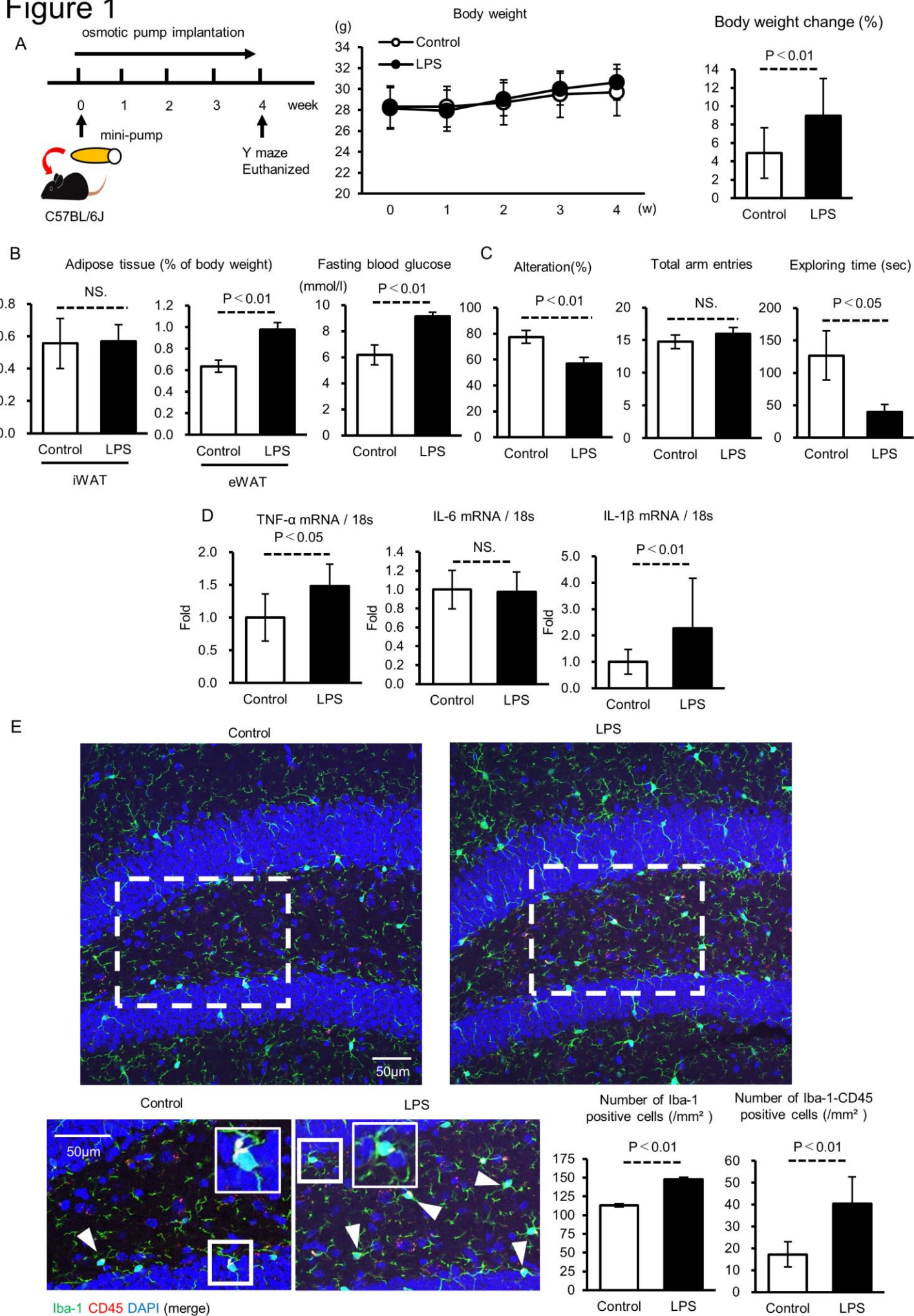
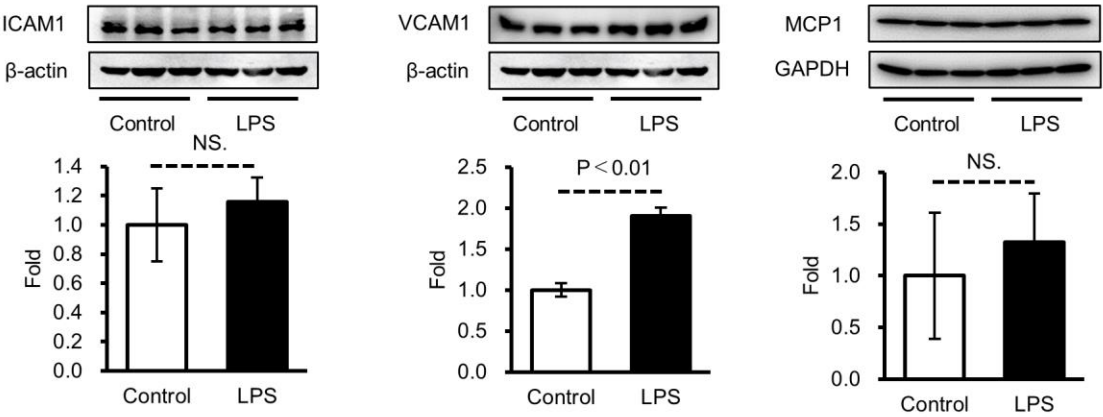
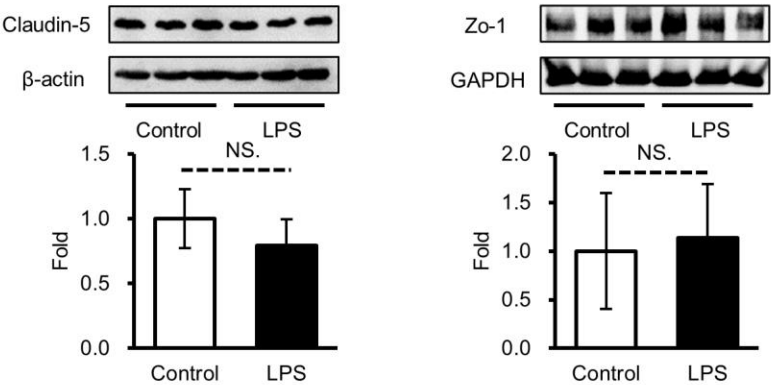


Figure 1 (Continued)

F



G



H

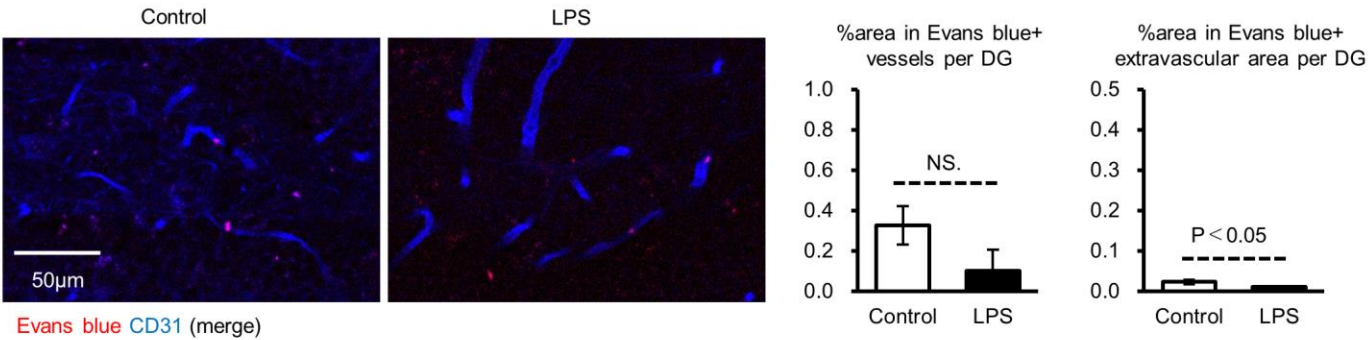


Figure 2

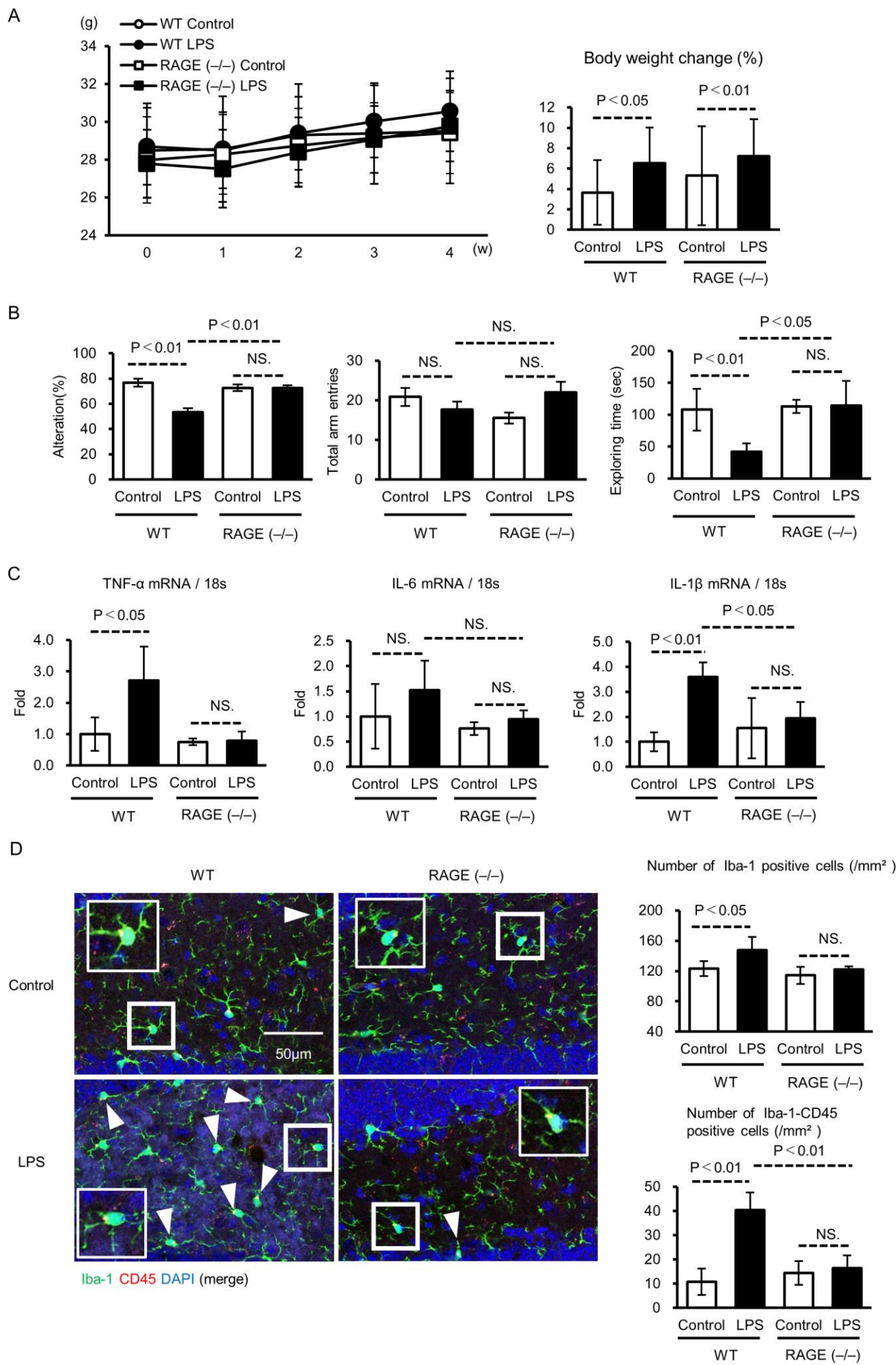


Figure 3

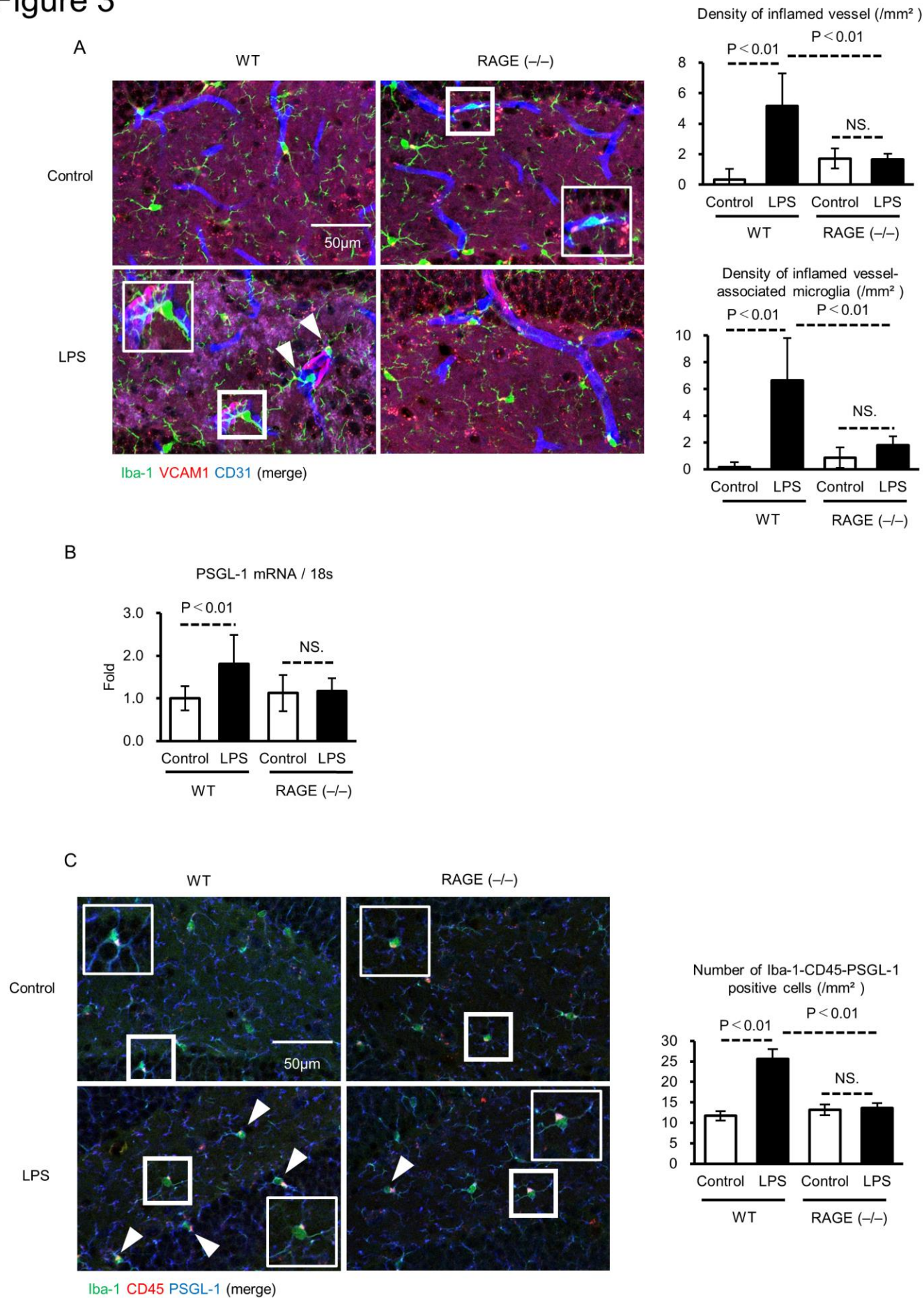


Figure 4

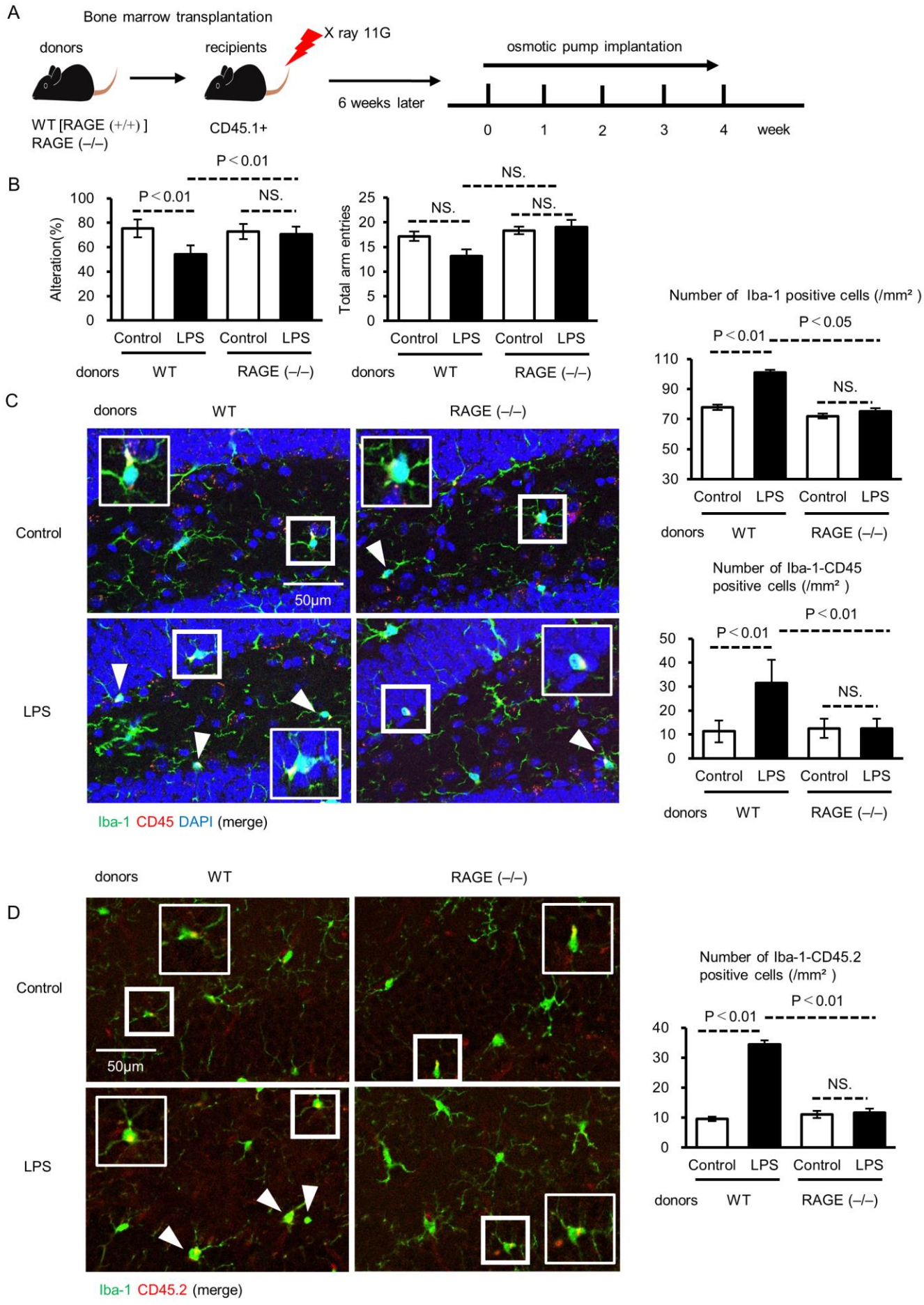


Figure 4 (Continued)

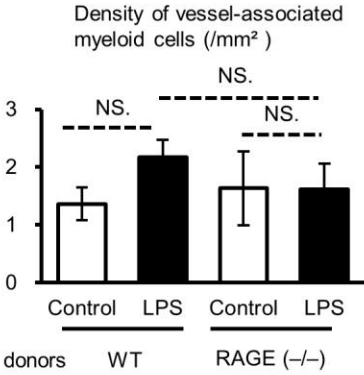
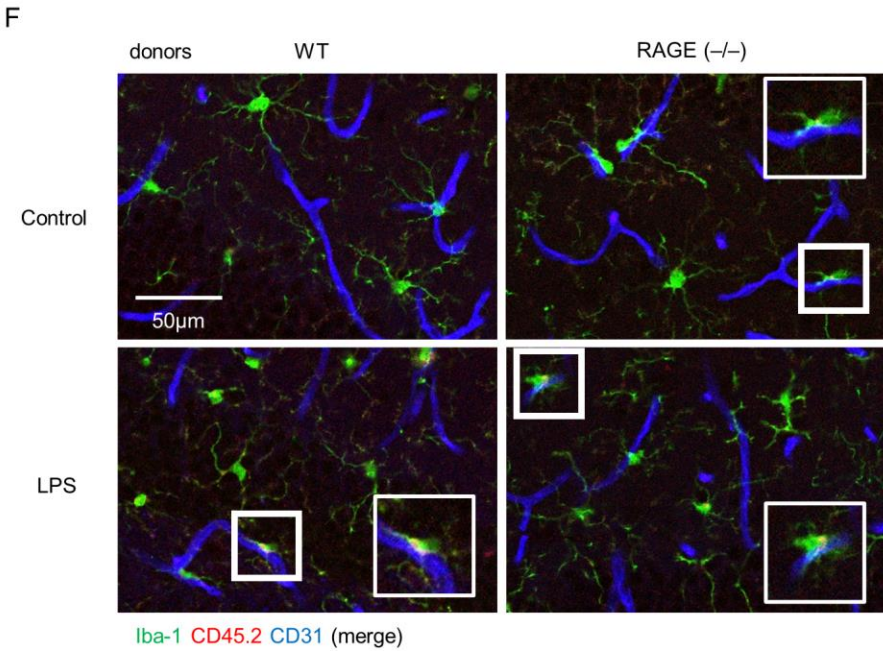
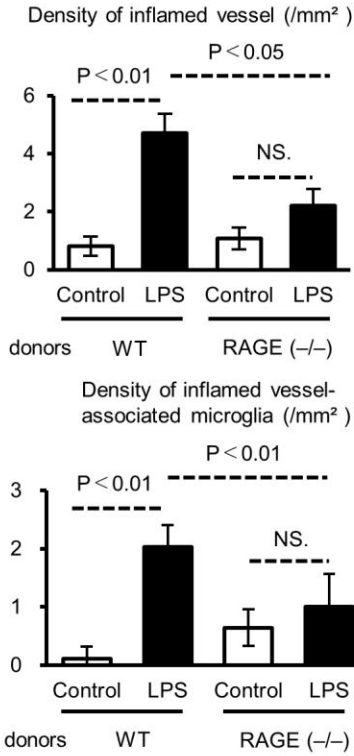
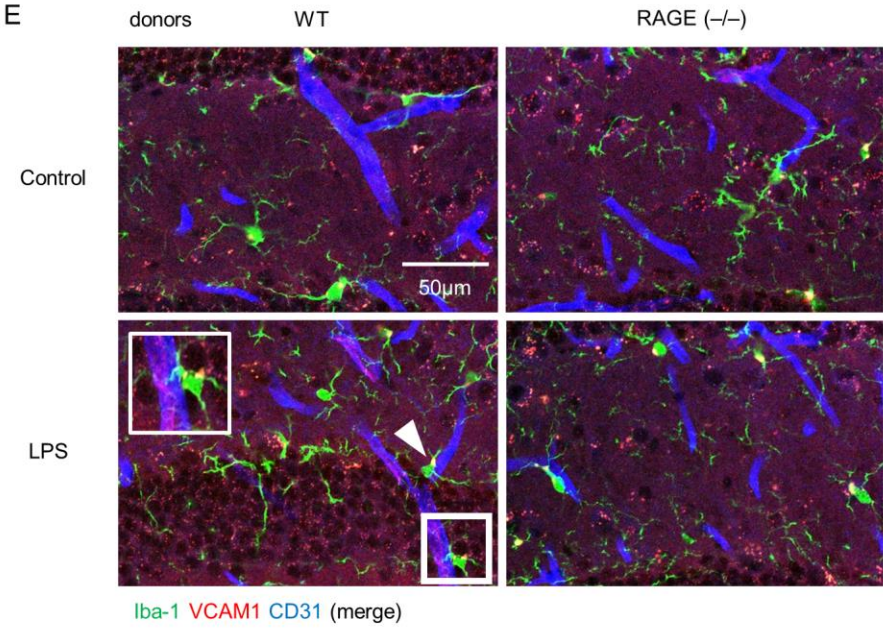


Figure 5

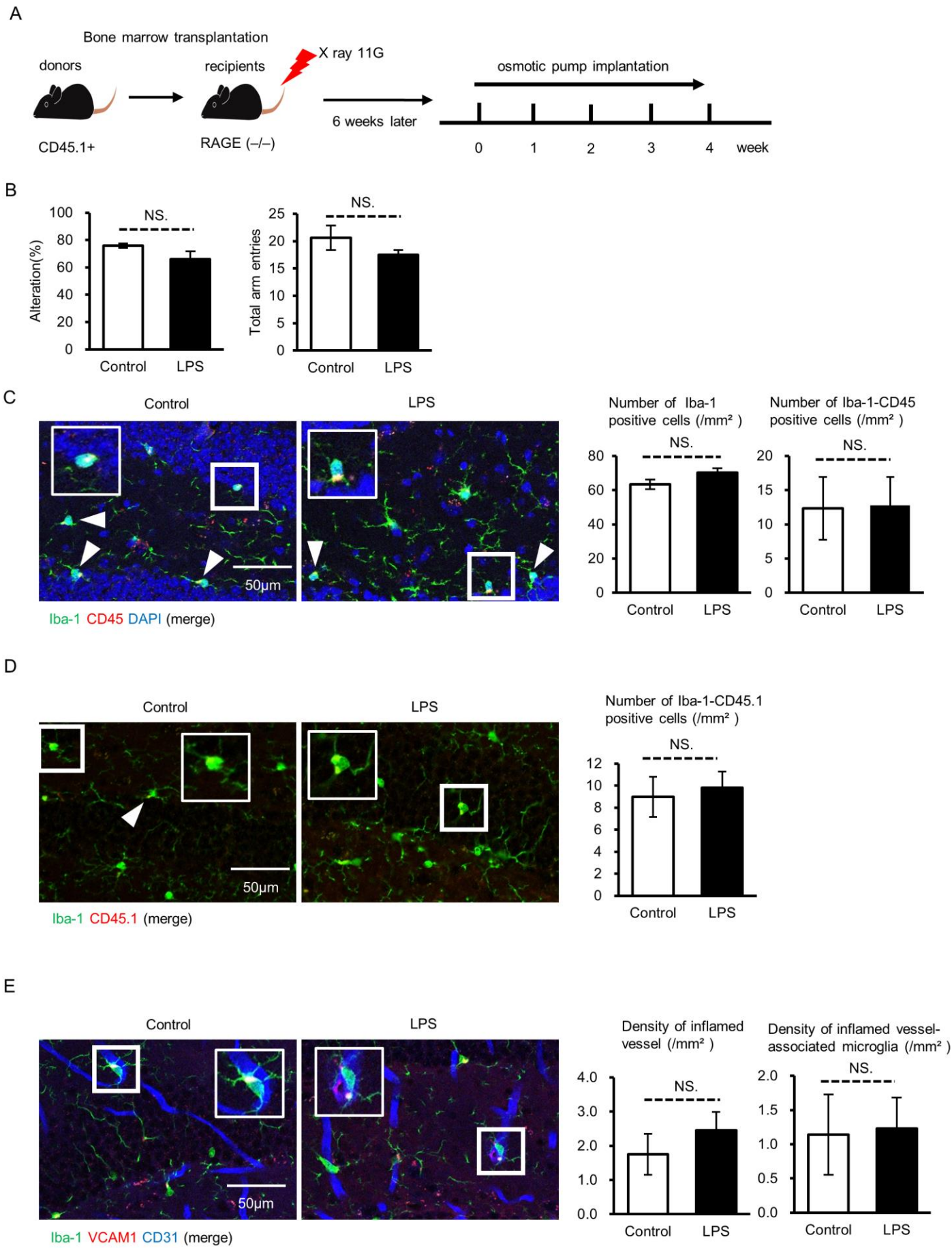
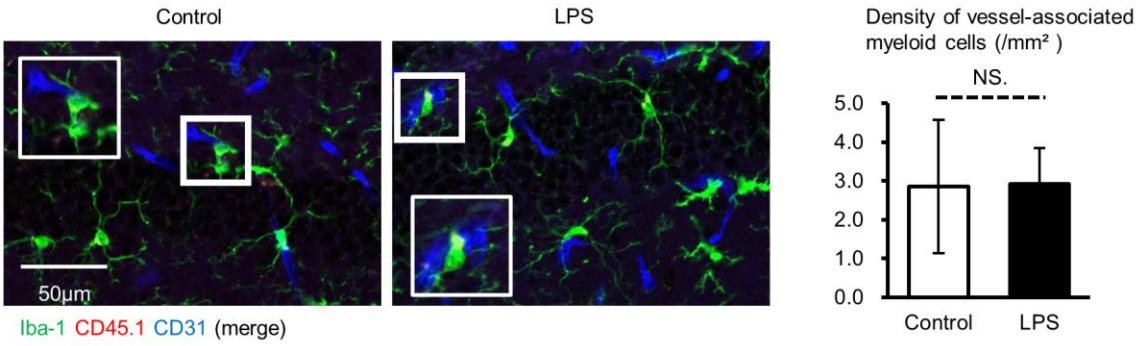


Figure 5 (Continued)

F



G

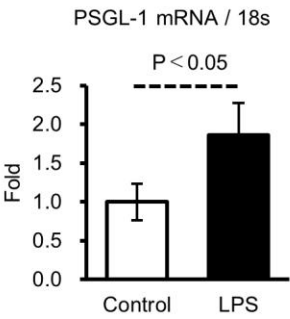
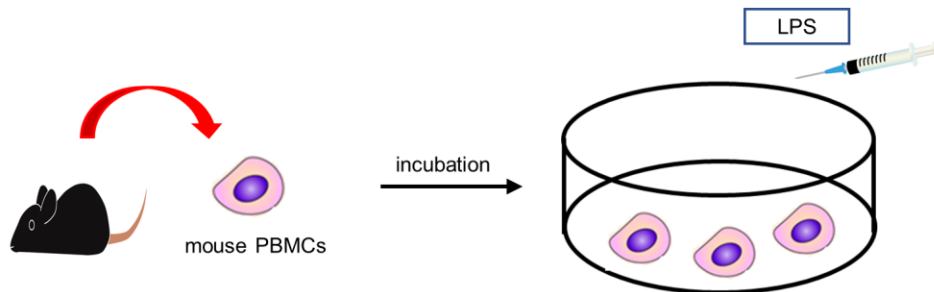
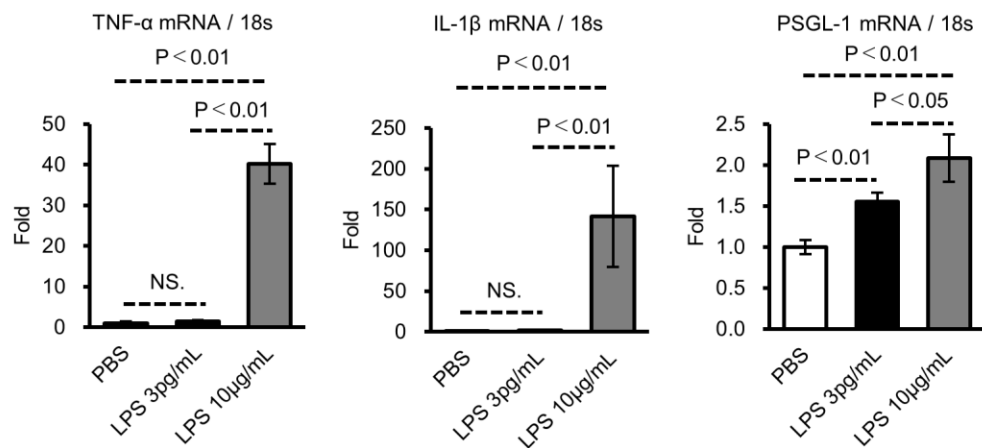


Figure 6

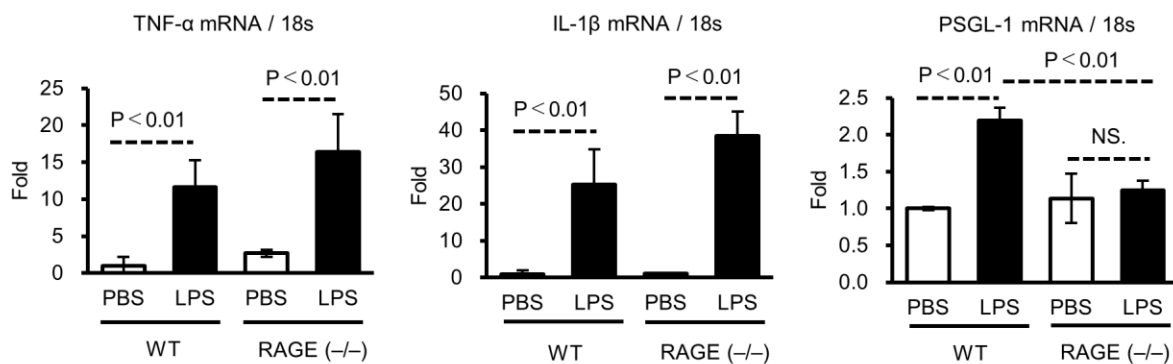
A



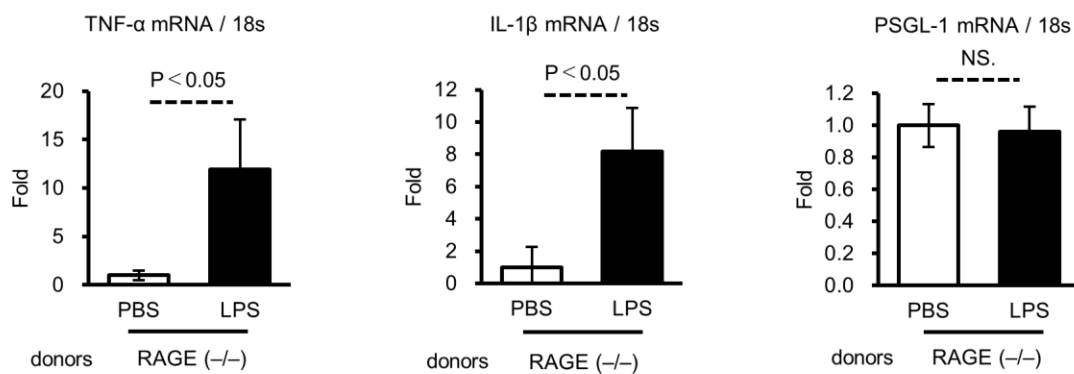
B



C



D



E

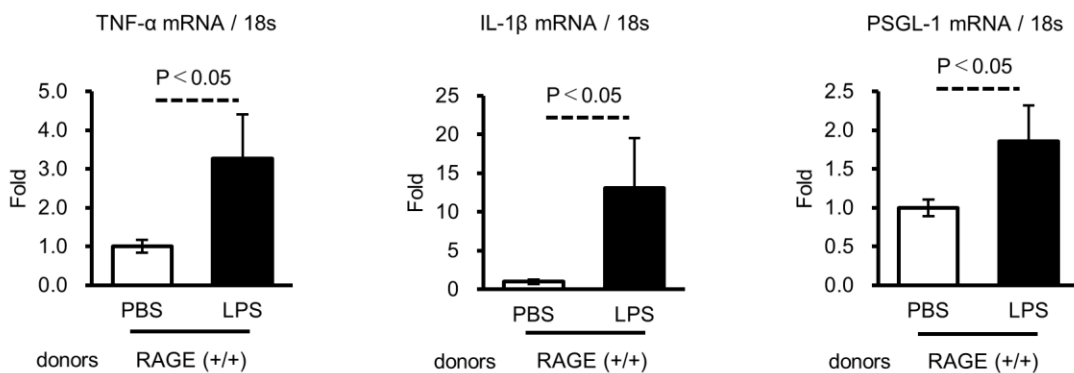


Figure 7

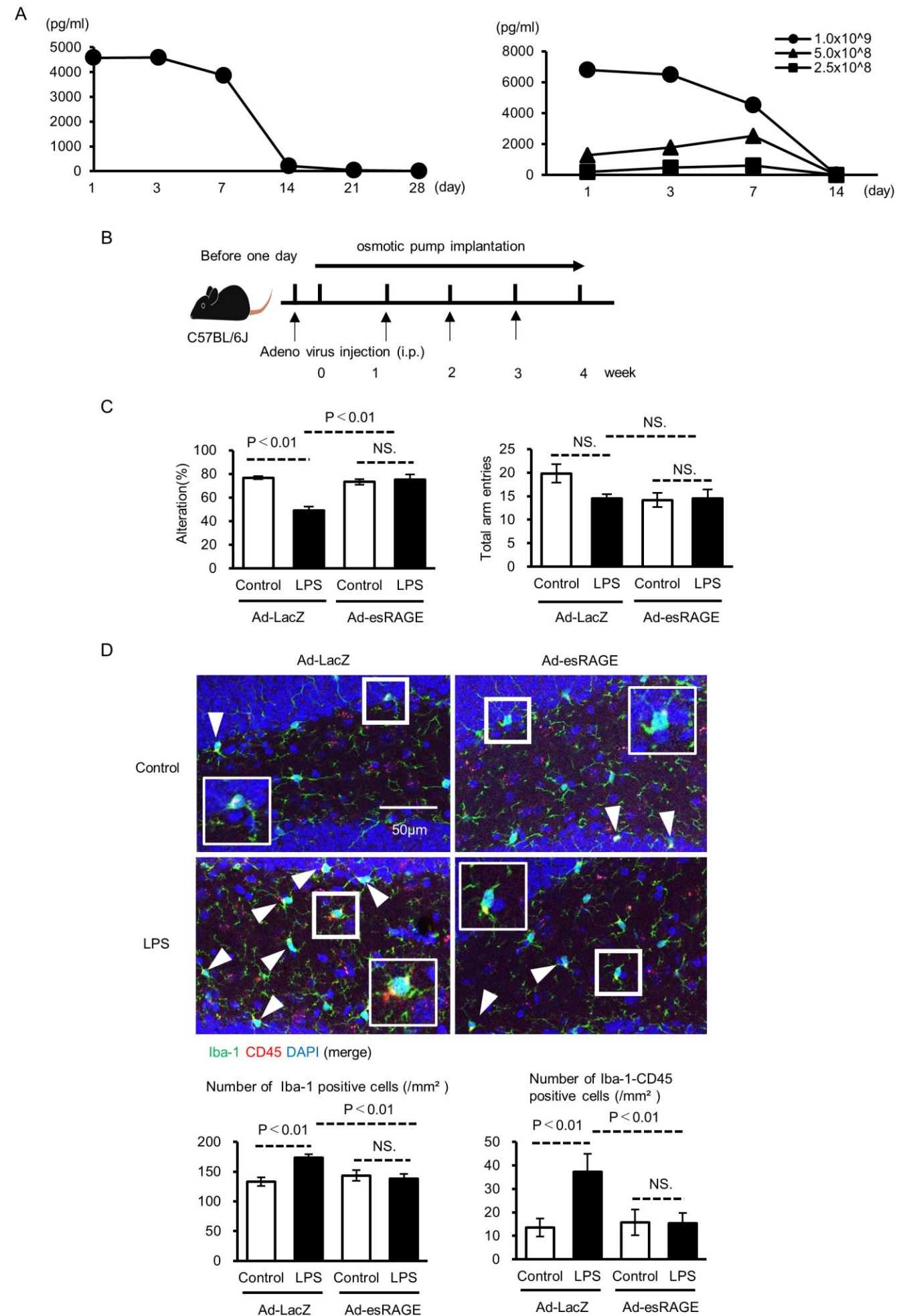
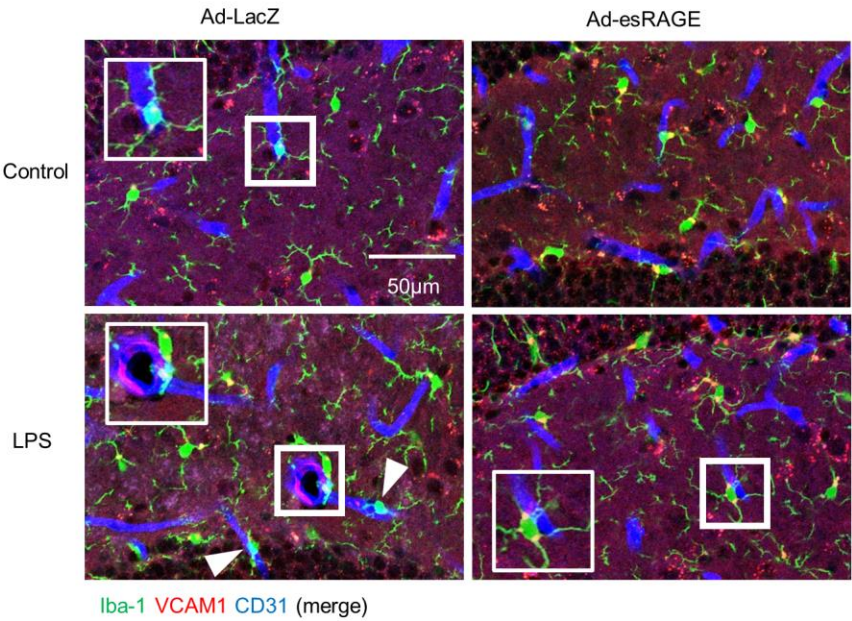
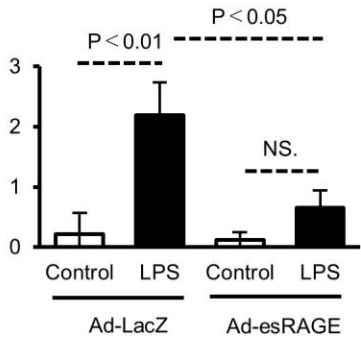


Figure 7 (Continued)

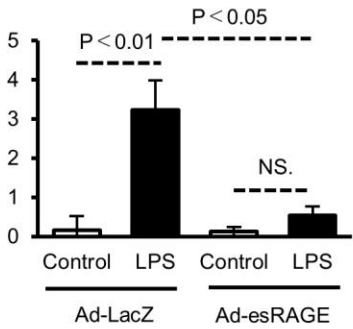
E



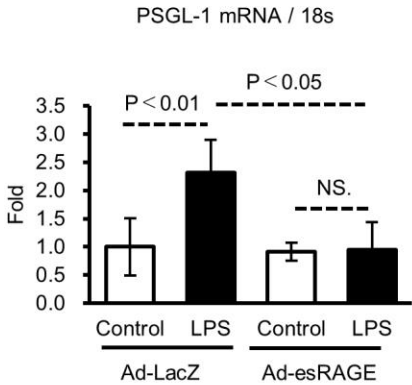
Density of inflamed vessel (/mm²)



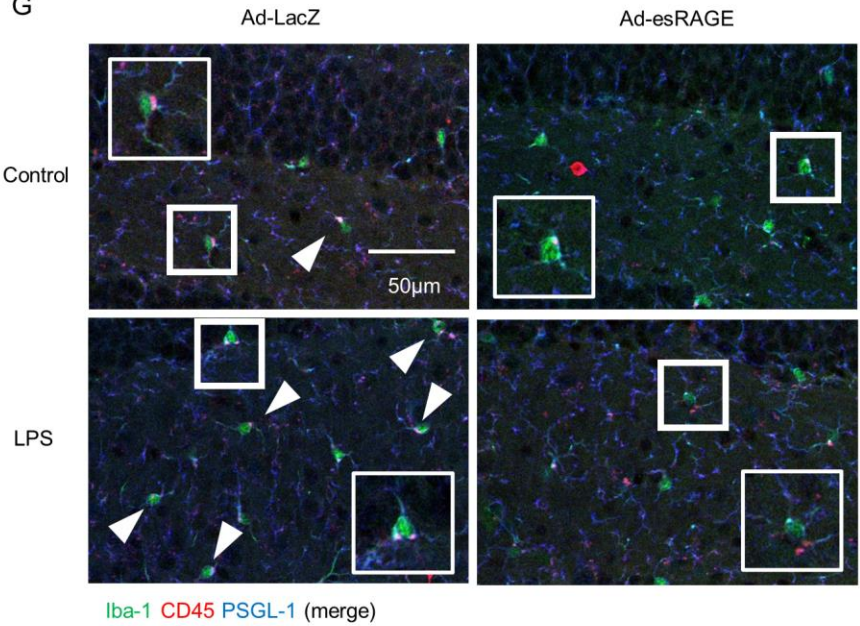
Density of inflamed vessel-associated microglia (/mm²)



F



G



Number of Iba-1-CD45-PSGL-1 positive cells (/mm²)

